The Johnstown Flood of July 1977: A Long-Lived Convective System

LANCE F. BOSART

Department of Atmospheric Science, State University of New York at Albany, Albany, NY 12222

FREDERICK SANDERS

Department of Meteorology, Massachusetts Institute of Technology, Cambridge 02139

(Manuscript received 17 December 1980, in final form 2 March 1981)

ABSTRACT

The heavy rains responsible for the disastrous flash floods near Johnstown, Pennsylvania, on the night of 19–20 July 1977 are shown to be part of a large quasi-circular mesoscale convective complex. This complex can be traced back to an origin in South Dakota nearly 96 h earlier. The complex tends to become more compact and intense during the night, with a radius of ~150 km, and to expand in response to new and peripheral convection during the day. On the small synoptic scale, the system is characterized by a pool of cool air at the surface and throughout the lower troposphere, just north of the centroid of the rainstorm, by a cyclonic circulation of substantial intensity in the lower and middle troposphere, and by anticyclonic circulation in the upper troposphere. Airflow relative to the moving storm is southeasterly at the surface, veering rapidly to southwesterly in the boundary layer and then to westerly in the upper troposphere.

Substantial convective instability is present throughout the environment of the storm, least in the northern sectors and greatest in the region of low-level inflow southwest of the centroid. A temporary reduction of this instability results in a weakening of the storm over the Great Lakes on the 18th, but a renewal of the supply of low-level heat and moisture is linked to a rejuvenation as the system approaches Pennsylvania. After crossing the Atlantic coast, the system is associated with a cyclonic circulation at the surface, which develops to tropical-storm intensity.

A study of the mass budget reveals prominent storm-scale ascent within 200 km of the rainfall centroid, compensated largely by descent in the annulus between the 200 and 400 km radii. Budgetary calculations over the storm area show that water vapor is made available principally by storm-scale convergence, with surface evaporation and moist horizontal advection playing smaller but by no means negligible roles. Convection removes the accumulating vapor long before large-scale saturation is reached, in a highly efficient process whereby nearly 90% of the water vapor made available by horizontal transport and surface evaporation falls as precipitation. The vertical motion and components of the water vapor budget are strongly modulated, but not entirely dislocated, as the storm passes through the region of strong diurnal low-level wind oscillation typical of the central United States in summer.

1. Introduction

The flash floods in and near Johnstown, Pennsylvania, on the night of 19–20 July 1977 took 76 lives and constitute a major recent meteorological disaster in the United States. We wish to show that the extraordinary rains in western Pennsylvania on that night were part of a large mesoscale convective complex that could be traced back over a 4-day period to an origin in South Dakota. We examine the small synoptic-scale disturbance in the flow pattern within which this complex was nurtured, identify the way in which water vapor was made available to the storm, and offer some speculations on how the larger rainstorm, not necessarily the Johnstown event itself, might have been inferred from the larger scale features.

2. The rainstorm

The history of the storm is illustrated by the maps of 12 h precipitation amounts appearing in Fig. 1, prepared from all available hourly raingauge data, while its character is revealed by the satellite imagery shown in Fig. 2.

Precipitation first became organized in South Dakota during the daytime period 1200 GMT 16 July to 0000 GMT 17 July, as see in Fig. 1a. The satellite view in Fig. 2 shows a cumulus complex of no great distinction. At this time an extensive earlier rainstorm covered much of the upper Midwest.

Twelve hours later (Fig. 1b) the South Dakota rainstorm has moved slowly eastward, while during this nocturnal period another intense storm has developed in Nebraska and has moved northeast-

0022-4928/81/081616-27$10.75

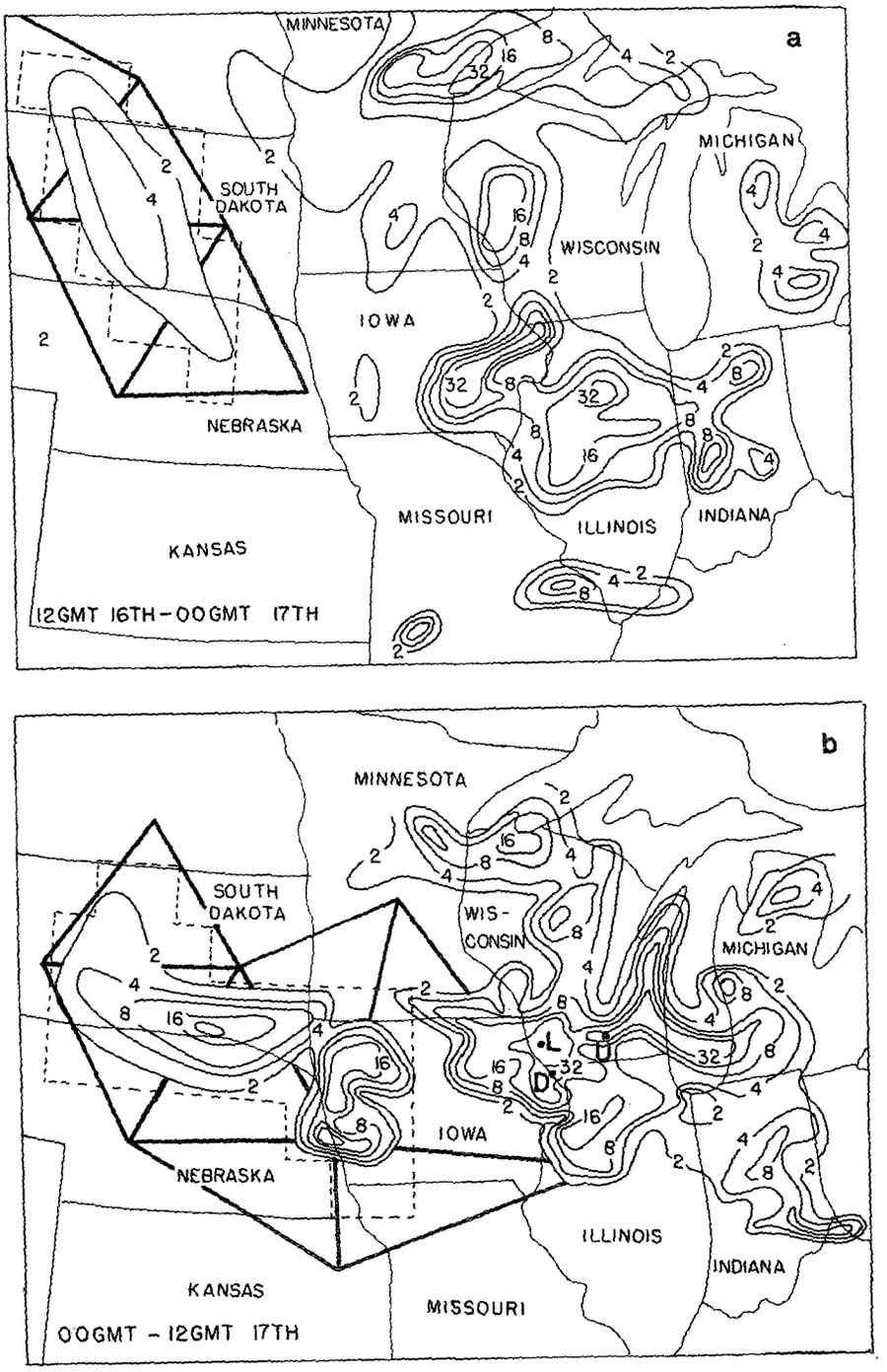

FIG. 1. Precipitation amounts for indicated 12 h periods, July 1977. Isohyets are for integer powers of 2 mm and are labeled in mm. The dashed line is the nominal outline used to determine the size of the rainstorm and its average intensity. The partially concealed heavy lines outline the triangles used in measurement of the water budget for the storm. Heavy dots and letters indicate locations of stations for which hourly precipitation amounts are shown in Fig. 3.

ward into western Iowa, joining the Dakota system. The satellite picture near the end of this period (Fig. 2) shows an extensive cirrus shield covering these two systems. The other, eastern, convective storm has made little progress.

During the following day, 1200 GMT 17 July to

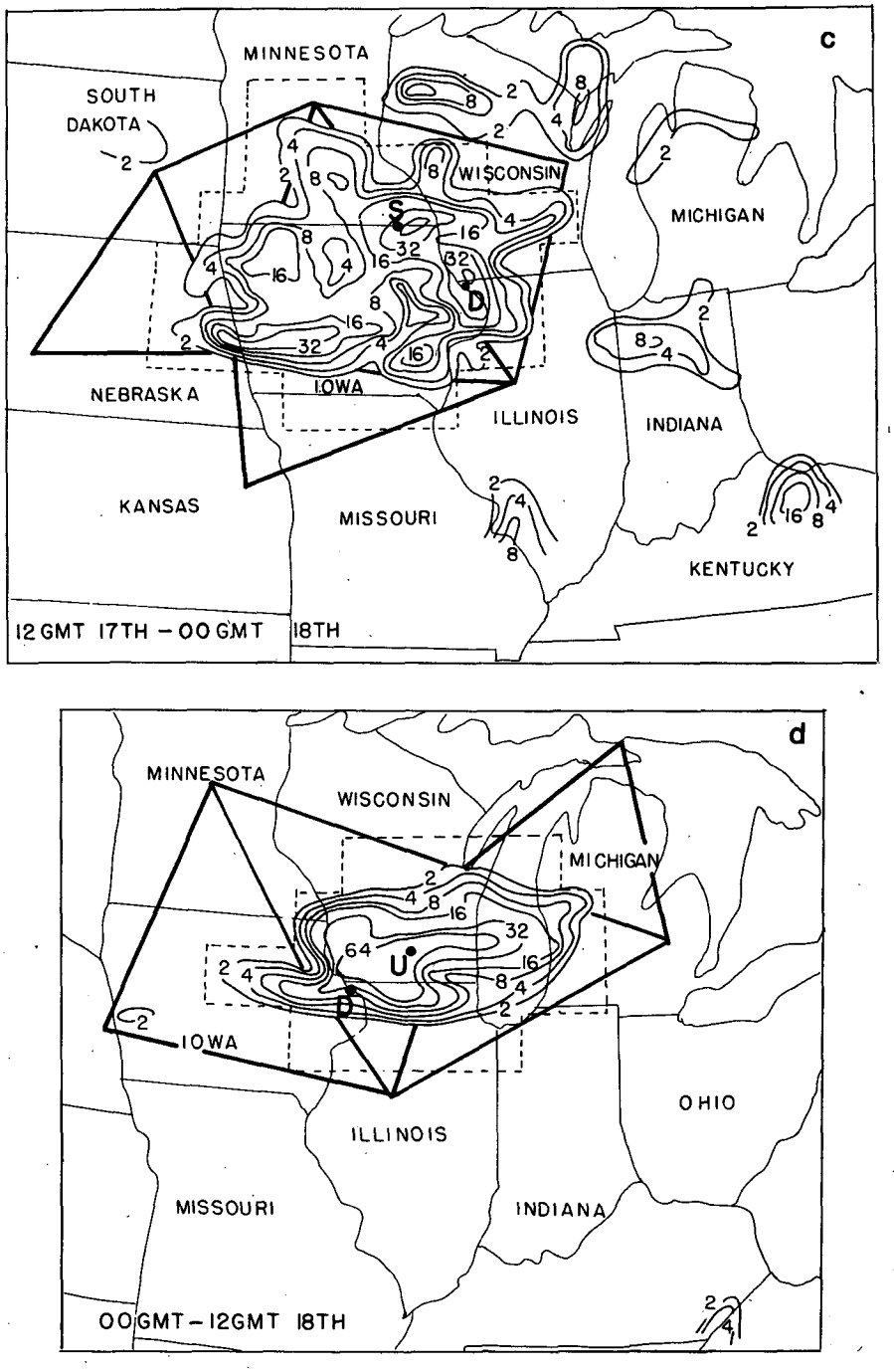

FIG. 1. (*Continued*)

0000 on the 18th, the eastern storm consists of only a few remnants, as seen in Fig. 1c, while the western system, still composed of a number of intense centers, moves to northeastern Iowa. The satellite picture shows dramatically the cirrus shield issuing from numerous active cumulonimbi.

A remarkable compaction of the storm occurs during the following night, 0000–1200 on the 18th (Fig. 1d), as the precipitation area, centered now in southern Wisconsin, shrinks but becomes more simply organized and intense. The cold high tops of the convective cloud mass, as viewed by satellite (Fig. 2), are impressive.

Then, during the following daytime period from 1200 GMT 18 July to 0000 GMT on the 19th, the system quickly becomes disorganized with the previous

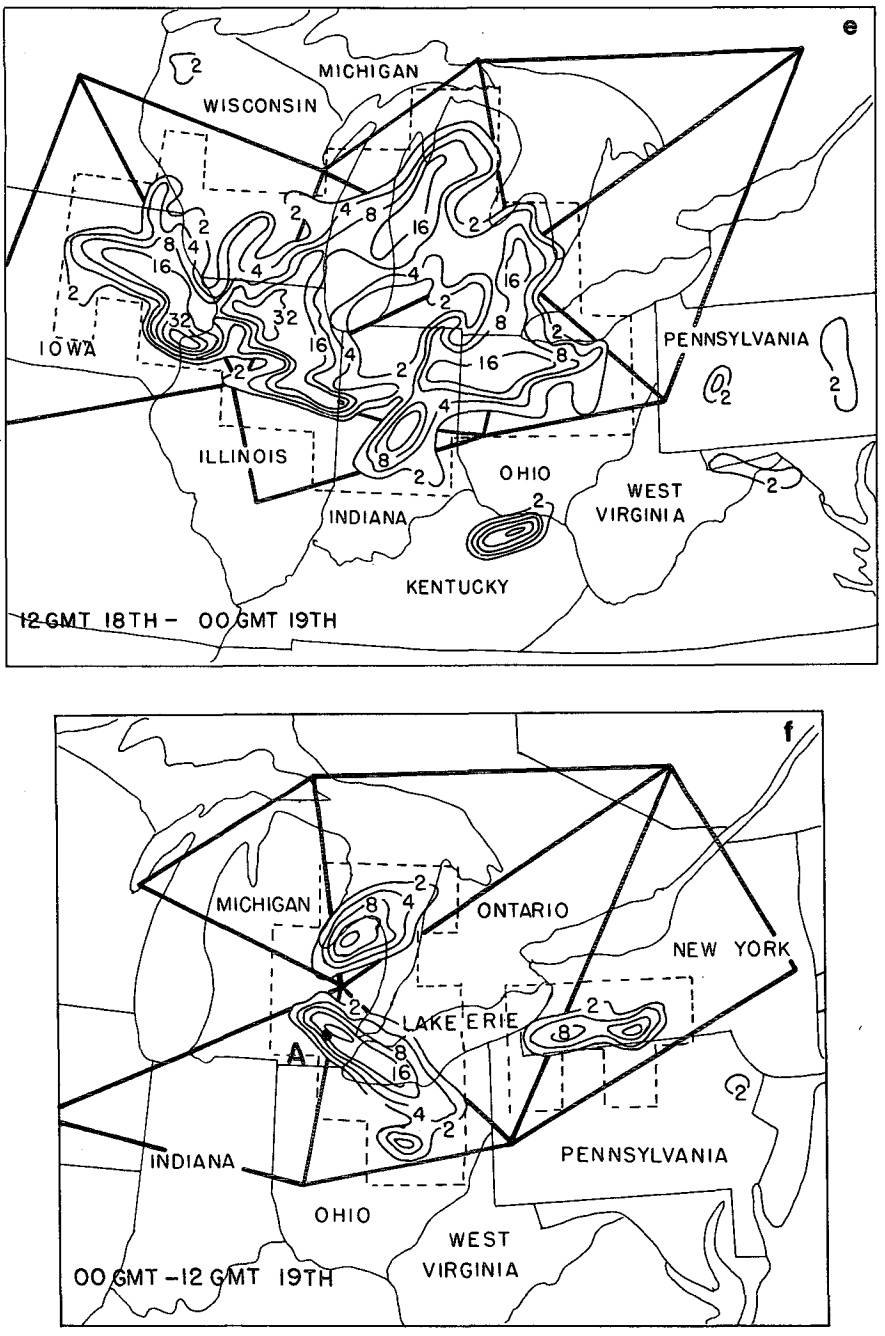

FIG. 1. (*Continued*)

nocturnal convection moving into lower Michigan and weakening, while vigorous new centers of rainfall appear in Iowa, Illinois, and Indiana (Figs. 1e and 2).

The nocturnal consolidation seen during the preceding night does not occur during the period from 0000 to 1200 GMT 19 July, as shown in Fig. 1f. Small centers of moderate to heavy intensity in Michigan, Ohio, and New York represent the complex in its weakest and least coherent state since initial organization. The satellite picture toward the end of the period, however, shows impressive thunderstorms, recently expanded over Lake Erie (Fig. 2) from a source in southeastern Michigan. Thus, the isohyetal analysis in Fig. 1f may err in showing no precipitation over most of the lake. In any event there is evidence of the reintensification to follow.

And follow it does during the day, 1200 GMT 19

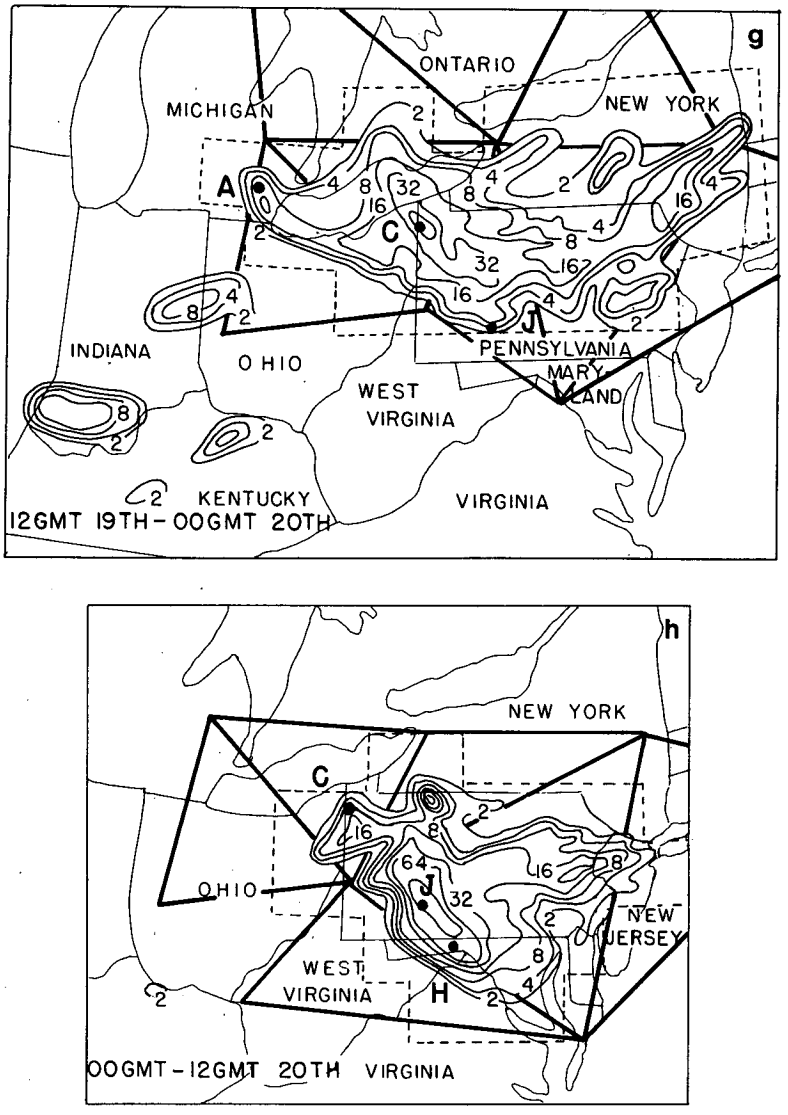

FIG. 1. (*Continued*)

July to 0000 on the 20th (Fig. 1g), as substantial precipitation is seen from southeastern Michigan to southern New York and almost all of Pennsylvania. Of particular interest is the northwest–southeast swath of extremely heavy rain from extreme northeastern Ohio to west-central Pennsylvania, emanating evidently from the near-dawn thunderstorm activity over Lake Erie. The southeastern edge of this swath has just reached Johnstown at the end of the period. Smaller daytime thunderstorm systems occur in Indiana, Ohio, and Kentucky (Figs. 1g and 2), as on previous days, representing deep afternoon convection which develops in the warm sultry air mass southwest of the main complex.

The flooding rains occur near Johnstown during the following night, 0000 GMT to 1200 GMT 20 July, as described in detail by Hoxit *et al.* (1978), and as shown in Fig. 1h. The storm, as it did two nights before over Wisconsin (Fig. 1d), becomes smaller but more intense. The aforementioned swath of extraordinarily heavy rain lies near the western edge of the complex and extends from west-central Pennsylvania across Johnstown into central Maryland. Scofield (1978) has shown how the IR satellite imagery (e.g., Fig. 2) reveals especially cold cloud tops in this area, confirming the heavy rain.

This account has shown some coarse differences between daytime and nocturnal behavior of the storm complex. A more detailed view of the diurnal behavior of the rainfall is obtained from Fig. 3.

West of the Great Lakes, precipitation was remarkably suppressed (Fig. 3a) between local noon (1800 GMT) and 6 pm (0000 GMT). Striking nocturnal maximum hourly amounts, shown in Fig. 3a,

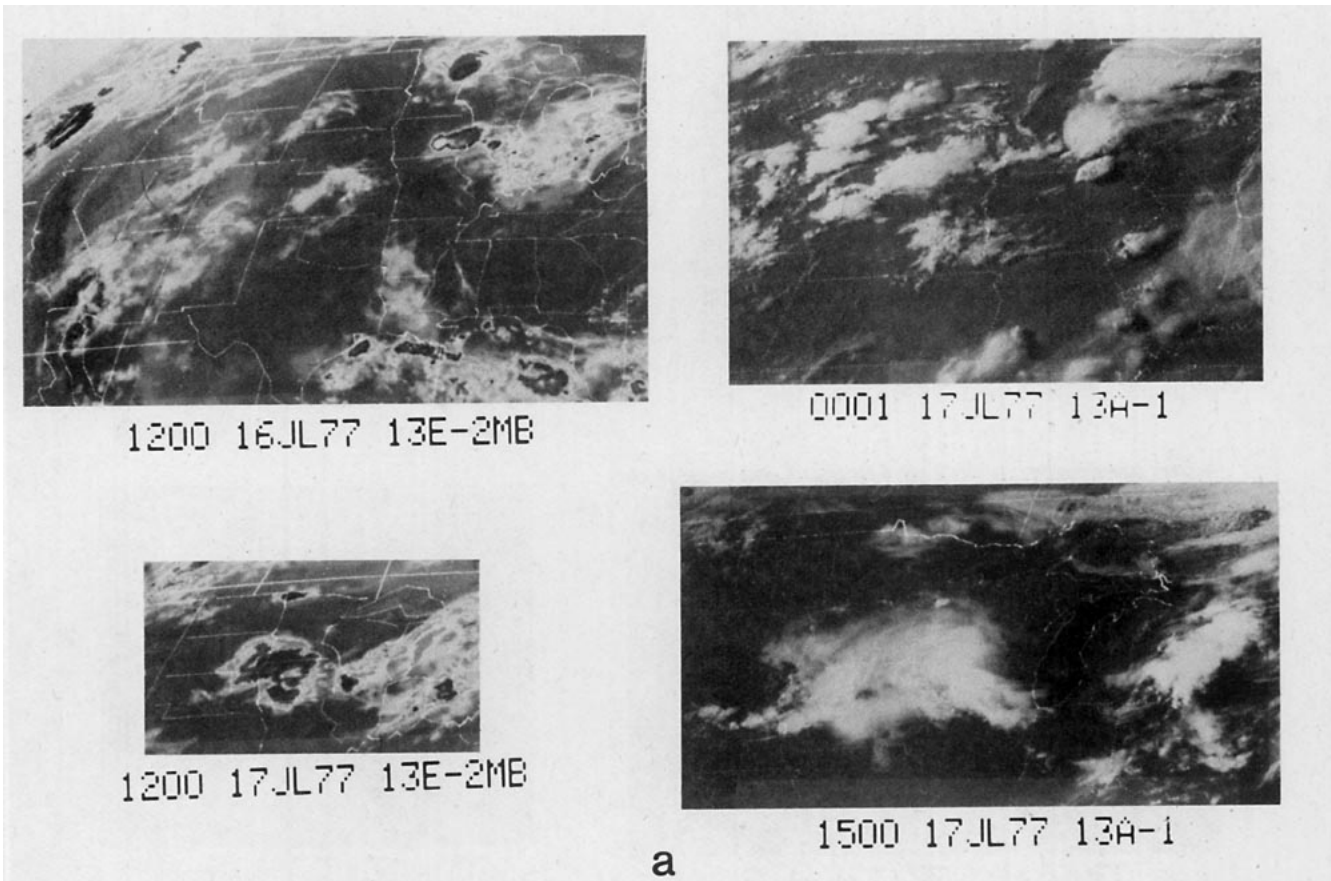

FIG. 2. GOES-E satellite imagery for times indicated.

fell in Iowa, Minnesota and Wisconsin between 2300 local (0500 GMT) and 0300 (0900 GMT), contributing to the large amounts appearing in Figs. 1b and 1d. Other impressive peak amounts occurring in the first few hours after sunrise at Spring Grove and Lancaster (Fig. 3a) contributed to the daytime amounts seen in Fig. 1c, but were evidently not the result of sustained heating and moistening of the surface boundary layer characteristic of daytime convection. Similar post-dawn convection, not shown in Fig. 3, contributed to large daytime amounts in eastern Nebraska and southwestern Iowa on the 17th (Fig. 1c) and again on the 18th in southeastern Iowa and central Illinois. This behavior is similar to that found by Maddox *et al.* (1979) to characterize flash floods of the mesohigh type.

Within and east of the Great Lakes region, afternoon suppression of convective rain was not evident, as hourly deluges began shortly after noon at Conneautville (Fig. 3b). This torrent, however, appears to be an inland continuation of convection initiated near sunrise over Lake Erie (Fig. 2). Heavy showers near dawn occurred also at Ann Arbor (Fig. 3b), contributing to 12 h amounts observed in both Figs. 1f and 1g. The rains at Johnstown began before sunset (Fig. 3b) but became catastrophic only after nightfall. Farther southeast, at Hancock Fruit Laboratory (Figs. 3b and 1h), the rain was nocturnal, with a final burst around sunrise.

The overall size and mean intensity of the rainstorm was determined for each 12 h period by identifying and counting the number of 1° latitude-longitude quadrilaterals in which at least 2 mm of rain fell in part of the area, and by estimating the area-average rainfall amount in each of these quadrilaterals. The result appears in Fig. 4. Growth of the area of the storm from the nocturnal period (0000–1200 GMT) to the following daytime period is seen in each instance. Shrinkage from day to night occurs except during the phase of initial growth on the 16th. Peak intensities are reached during the nighttime periods 0000 to 1200 GMT on 18 and 20 July, the latter of these periods producing the Johnstown floods. Approximately 18×10^{12} kg of water reached the ground over the 96 h period.

3. The synoptic patterns

The large-scale environment of the convective rainstorm is one of weak flow, but hardly one devoid of interest, as we will see. The surface situation at the inception of the storm is illustrated in Fig. 5. East of the Rockies a typical westward extension

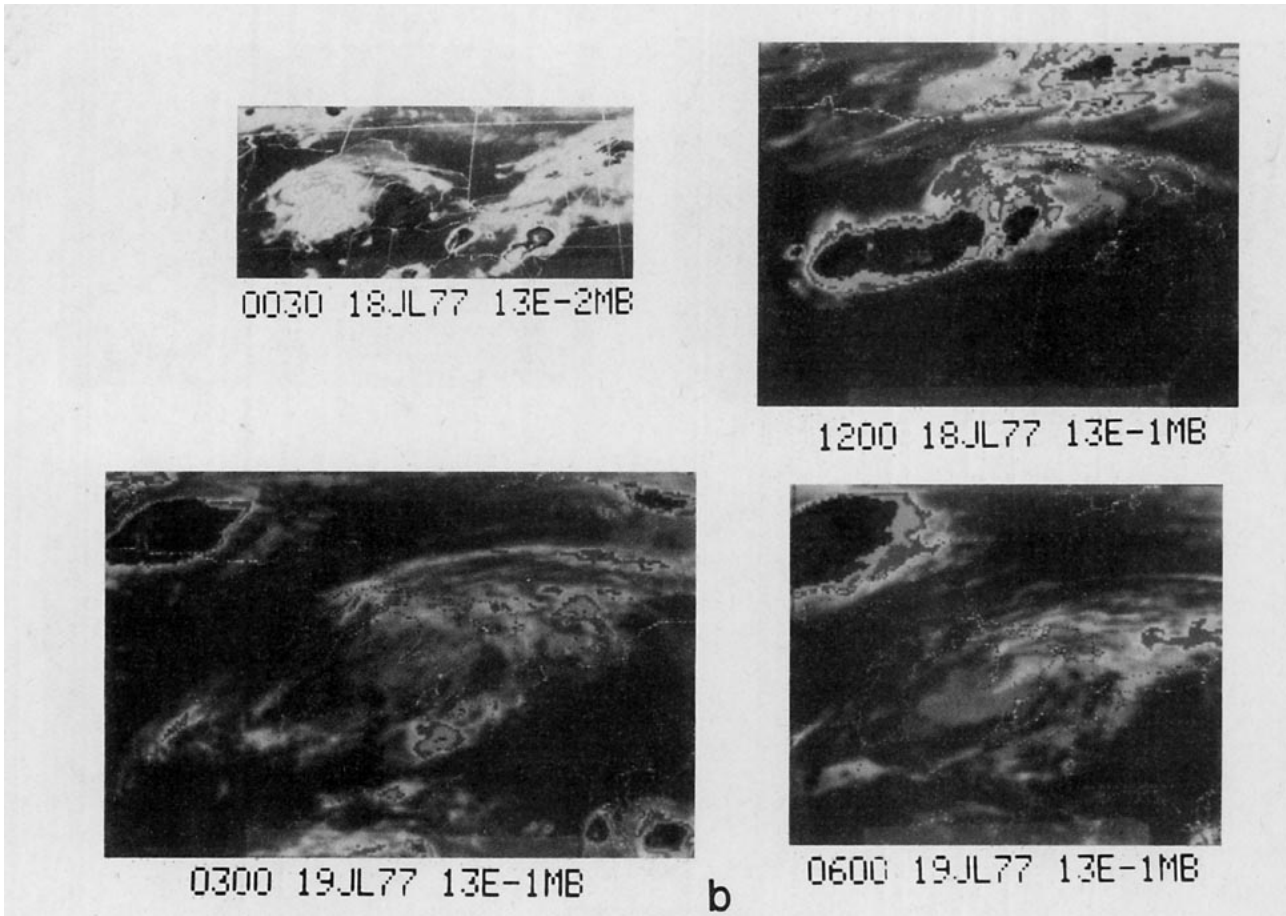

FIG. 2. (*Continued*)

of the anticyclonic flow around the Bermuda high has brought a flood of warm humid air over virtually the entire United States east of the Rockies. A typical weak trough of low pressure lies immediately east of the mountains. Showers in this trough in western South Dakota represent the beginning of the convective system. The front through the midwest marks the southern edge of the pool of cooled air produced by convection in the eastern system.

At upper levels (Fig. 6) the main belt of temperature contrast and associated westerlies lies well to the north of the convection, in southern Canada. In the northern plains of the United States there is strong warm advection at 850 mb downwind from the elevated hub of heated air over the mountains. At 500 mb a weak trough line in the wind flow is associated with the eastern convective system along the border between South Dakota and Minnesota. In the upper troposphere a meridional temperature contrast across the northern plains is reflected in a secondary jet at 200 mb across South Dakota. This jet is bounded to the northwest by a trough, oriented west-southwest to east-northeast, and may be linked to the initiation at convection in the manner suggested by Uccellini and Johnson (1979).

The evolution of the surface pattern up to the time of beginning of the heavy rains near Johnstown is seen in Fig. 7. There is little substantial perturbation of the synoptic-scale pressure pattern, although in the regions where convection maintains a pool of rain-cooled air the pressure is slightly elevated. This association is least well organized between 0000 and 1200 GMT on the 19th (Fig. 7c and 7d), when the rainstorm becomes temporarily dispersed (cf. Fig. 1f).

The upper level sequence during the same period appears in Fig. 8. The most striking feature at 850 mb is the relatively cold pool which develops, in the face of warm advection, to the north of the centroid of the convective storm after 1200 GMT of the 17th, and moves with the storm thereafter. This cool air is evidently a by-product of the convection. A developing cyclonic circulation bounds the cold air on the south.

At 500 mb there is no evidence of this pool. However, a trough is first seen (Fig. 8a) west of the centroid of the storm. The initial sign of it, in fact, is a south-southwest wind in western South Dakota at 0000 GMT on the 17th, decidedly west of the developing convective system. By 1200 GMT on the 18th, the end of the period of the intense and compact

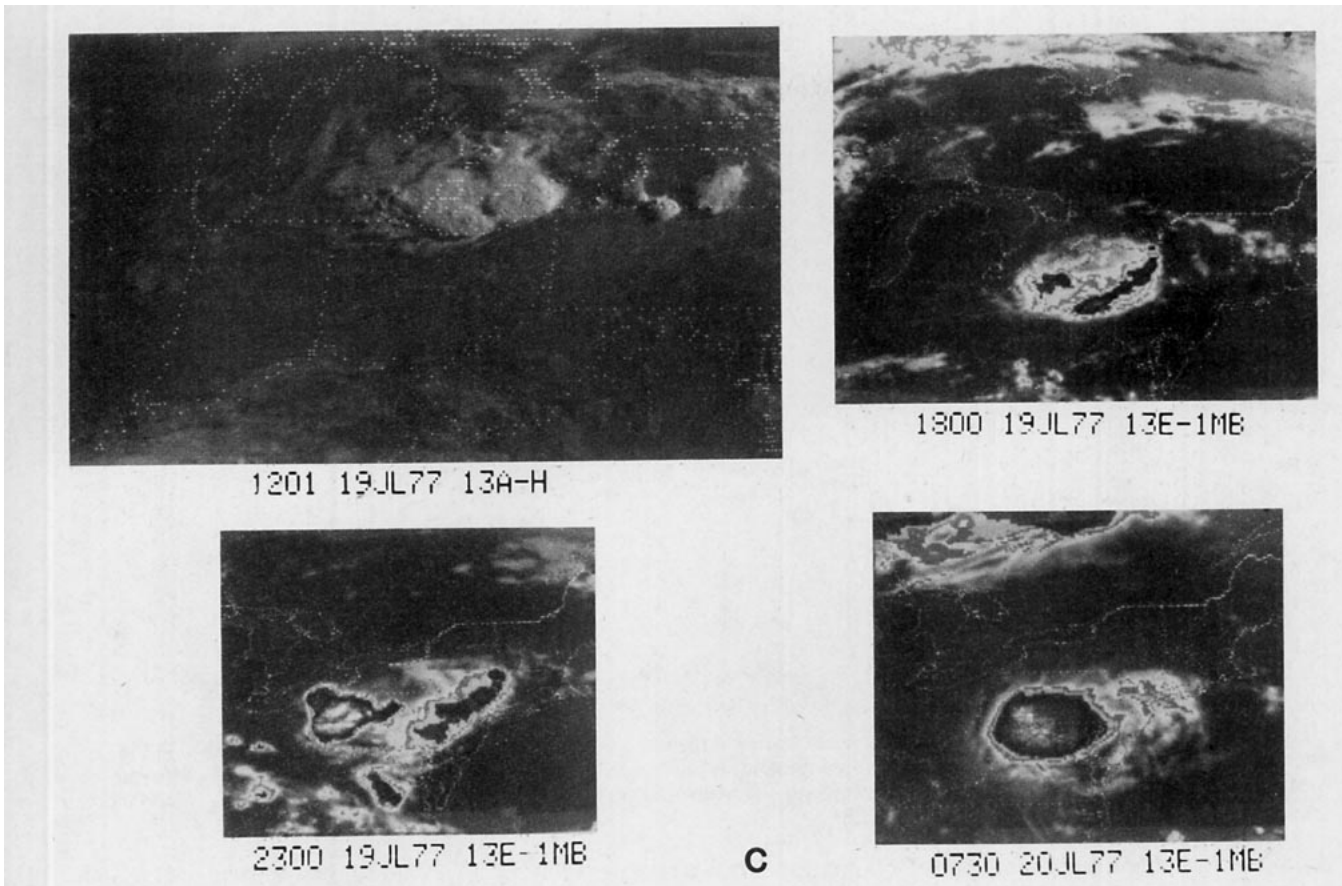

FIG. 2. (*Continued*)

rainstorm shown in Fig. 1b, this trough is nearly coincident with the centroid and shows a more pronounced cyclonic circulation, centered close to the 850 mb cold pool. Thereafter, a pronounced 500 mb trough is continuously evident. On the 19th, when the rainstorm is not well organized, the trough lies northwest of the centroid, but then the two come back into coincidence when the compact, intense, and disastrous rainstorm begins over Pennsylvania (Fig. 8e).

In the upper troposphere the flow patterns are quite different. The centroid of the storm lies consistently to the east of a 200 mb trough, which appears to be a westward-displaced counterpart of the 500 mb trough. The storm in fact, although forming near the 200 mb jet in South Dakota (Fig. 6c), is thereafter closely associated with a ridge line. The anticyclonic circulation over the storm at 200 mb is especially pronounced at the outset of the Johnstown episode (Fig. 8e), when a closed center appears in Pennsylvania, embedded in a ridge of larger scale. This mesoscale high is an example of the type discussed by Fritsch and Chappell (1980).

The surface map at the end of the Johnstown storm appears in Fig. 9. A warm humid circulation still covers almost all of the central and eastern United States. A cold front has invaded the northern plains. Remnant showers and thunderstorms continue in a weak trough in the lee of the Appalachians. Aloft (Fig. 10) we see little change in the broad-scale situation. In the major belt of westerlies a ridge has advanced in the four days from western Canada to a position just east of Hudson's Bay. In the northern plains the initial 200 mb jet has disappeared, while the cyclonic circulation described above has developed at 850 and 500 mb. The track of the centroid of the convective storm, and of the associated 500 mb trough, appears to have been steered by the large-scale mean flow in the middle troposphere. In many ways, the upper level features resemble those shown by Maddox *et al.* (1979) to characterize midsummer flash floods.

4. Analysis of soundings

At each observation time from 0000 GMT on the 17th to 1200 GMT on the 20th, the soundings within 300 n mi (554 km) of the centroid of the rainstorm were assembled. An average of the temperature and humidity structure of the 54 soundings for the en-

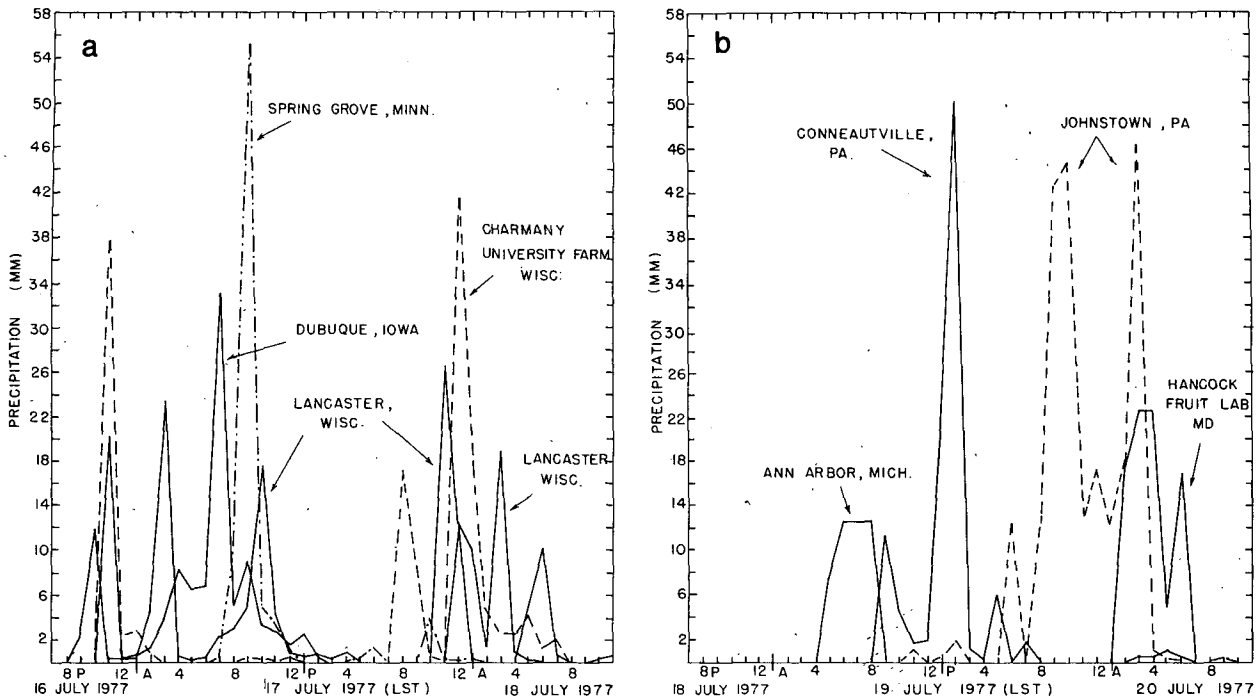

FIG. 3. Time series of precipitation amounts for hours ending at the indicated times. Locations of the stations are shown in Fig. 1, where D refers to Dubuque, Iowa; S Spring Grove, Minnesota; L Lancaster, Wisconsin U Charmany University Farm, Wisconsin; A Ann Arbor, Michigan; C Conneautville, Pennsylvania; J Johnstown, Pennsylvania; and H Hancock Fruit Laboratory, Maryland.

tire period for the layer from 850 to 100 mb appears in Fig. 11. For each sounding, the point with highest equivalent-potential temperature in the layer below 850 mb was lifted dry adiabatically to saturation and then moist adiabatically to 500 mb, where its temperature was subtracted from the ambient value. The mean of the difference, with its associated moist adiabat, seen in Fig. 11, shows substantial convective instability above a level of free convection near 700 mb.

The time evolution of the area-mean sounding is shown in Fig. 12, with an average of four soundings added for 12 GMT on the 16th in the region of initial development of the storm. Until 1200 GMT on the

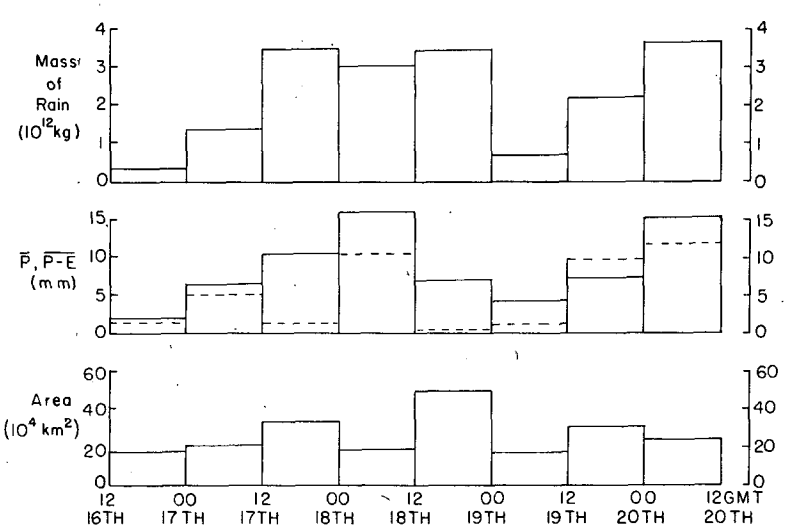

FIG. 4. Summary of size, mean intensity ($\bar{P}$) and total amount of the rainstorm for indicated 12 h periods and for the outlined areas in Fig. 1. Diagnosed mean precipitation minus evaporation, $\overline{P-E}$ from Table 2 is shown by the dashed lines.

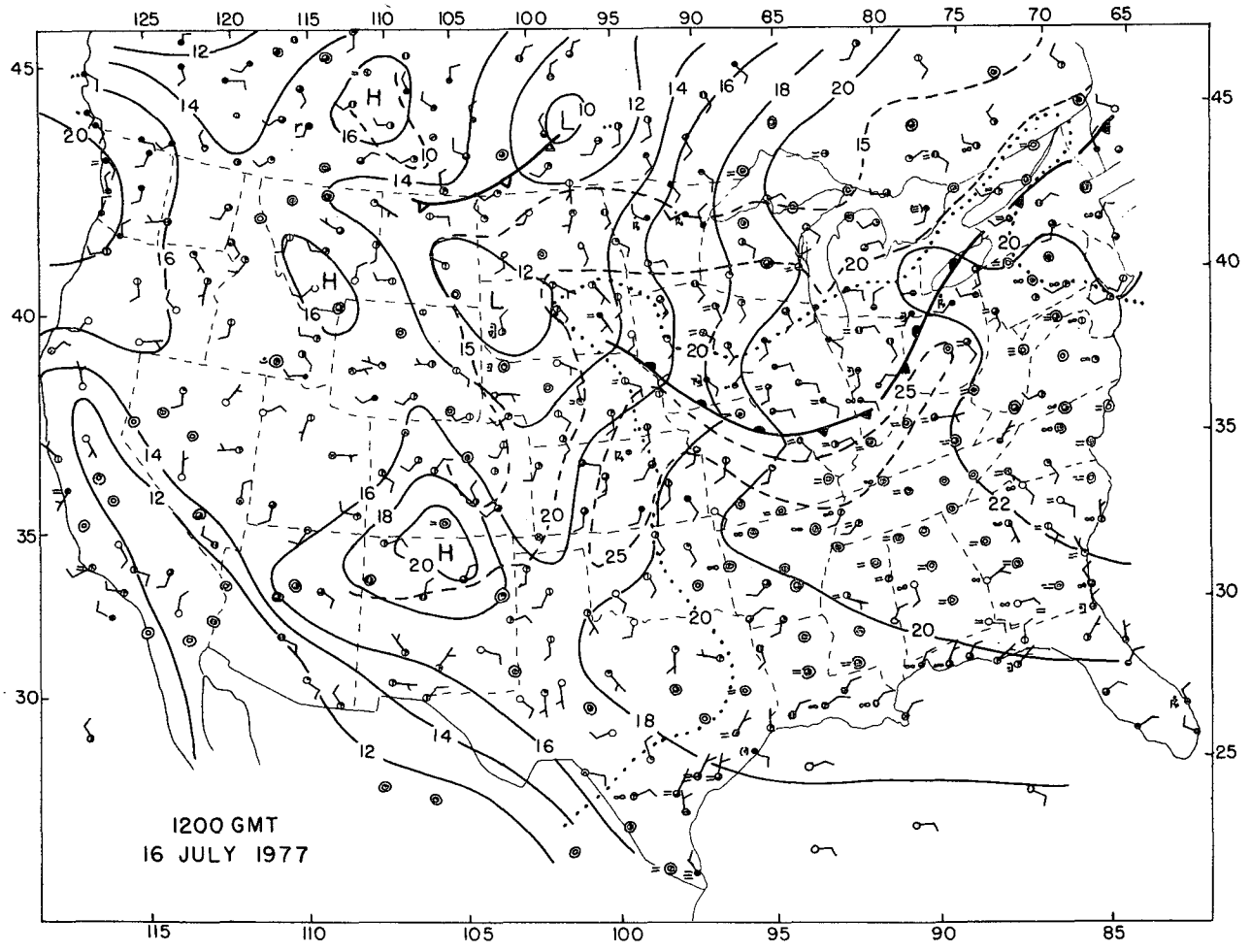

FIG. 5. Surface map, with selected elements plotted according to the conventional model. Isobars of sea level pressure are labeled as the excess (mb) over 1000 mb. Dashed lines are isotherms, labeled in °C. The dotted line is the 20°C dew-point isotherm.

18th the area-mean sounding becomes cooler and moister below 500 mb and warmer from this level to 200 mb. The tropopause region cools as the storm develops. There is a large diurnal variation of convective instability, shown by the lifted moist adiabat, as the layer below 850 mb provides larger values of equivalent potential temperature at 0000 (in the early evening) than at 1200 (shortly after sunrise). The source of the lifted parcel is almost always at or near the surface at 0000 and is characteristically about 50 mb above at 1200. The importance of the diurnal heating and cooling of the surface boundary layer seems clear.

We note from Fig. 12c that the convective instability is markedly least at 1200 GMT on the 18th and that it has been only modestly restored 12 h later. The period following these soundings is characterized by near dissolution of the storm, as discussed previously. The period from 0000 to 1200 GMT on the 19th is the only night during which the instability increased, foreshadowing the regeneration of the storm as it approaches Pennsylvania. Evidently, the system requires substantial instability for its maintenance.

The soundings were stratified, without regard to time, according to their azimuth sector relative to the track of the storm. Mean soundings in Fig. 13, show that the instability is least in the left sectors, particularly the forward one, and is the greatest in the right-rear sector, where maximum inflow is occurring.

For each sector and range, the deviation of the mean soundings of temperature and relative humidity from the grand means (Fig. 11) was obtained. Resulting values at each standard pressure level are mapped in Fig. 14. Relatively cool air at 850 and 700 mb is seen to encompass the interior region of the storm, with a cool center just to the left of its path. From 500 to 200 mb the temperature patterns are less well defined, but cooler air lies to the left rather than to the right of the path, and the interior region of the storm is warmer than the environment.

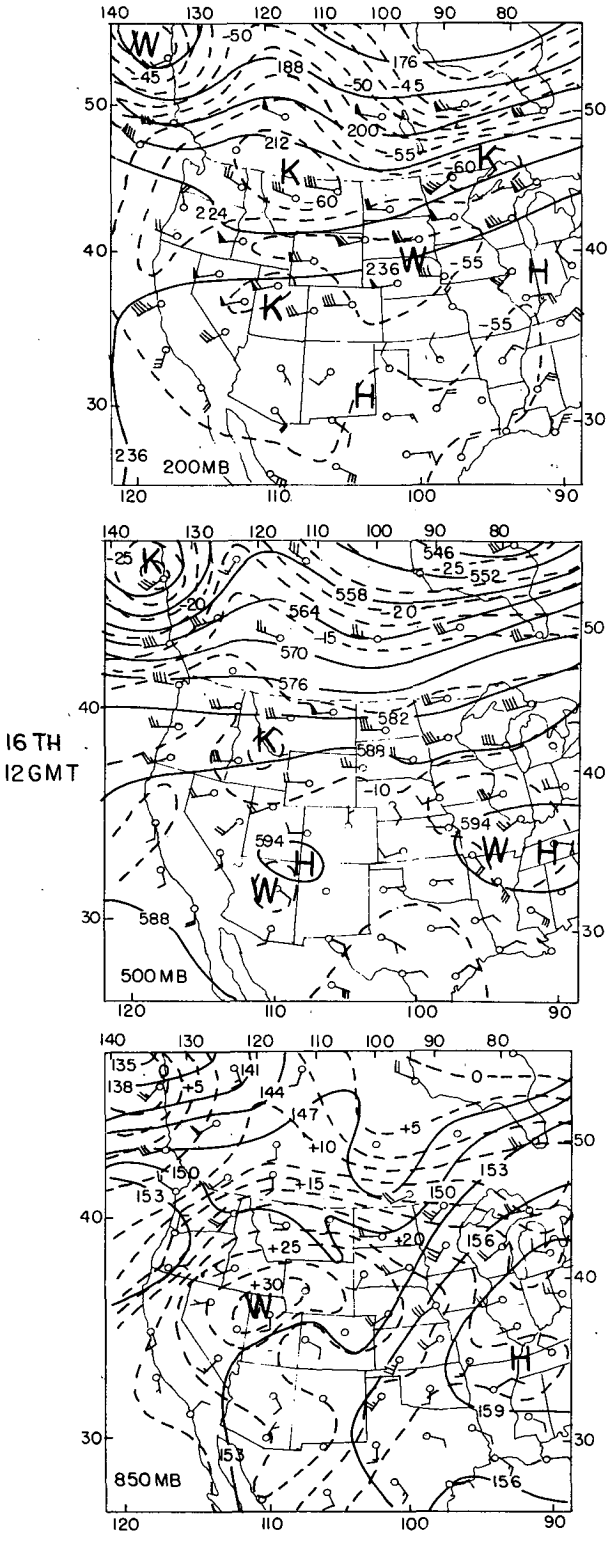

FIG. 6. Upper level charts for indicated constant-pressure surfaces with winds plotted in the usual convention. Dashed lines are isotherms at intervals of 2.5°C, with temperature maxima and minima denoted W and K, respectively. Solid lines are height contours, at intervals of 3 dam at 850 mb, 6 at 500 mb and 12 at 200 mb.

In the lower stratosphere there is a substantial temperature decrease from the left-rear to the right-front sector.

A center of relatively moist air appears in Fig. 14b near the storm centroid at 850 and 700 mb, and somewhat to the left from 500 mb to the upper limit of humidity information. Relatively dry air characterizes the outer environment at 700 mb in all but the left-front sector. At 500 and 400 mb, dry air is present in the right sectors near the rainstorm centroid.

The overall structure indicates that vigorous convection is initiated mainly in the right-rear sector with moist unstable air below and dry air aloft. The instability is nearly exhausted in the left-front sector but cloud debris persists in extensive layers of middle and high clouds in both left sectors.

The wind data in the 54 proximity soundings were analyzed in greater detail. At each standard level, and at 900 mb, the range of each observation from the centroid of the rainstorm was determined, together with its azimuth relative to the direction of propagation of the storm. The resulting data set, at 900 mb, is shown in Fig. 15 as an example.

Manual analyses of the tangential and radial velocity components, relative to the centroid, were performed at each level. From these, values were estimated at each 10° of azimuth and at distances of 1.5, 2.5, 3.5 and 4.5° of latitude (166, 277, 389 and 499 km). Values at relative azimuths of 360° through 080° were averaged to yield values for the left-front sectors. Mean values for the other three sectors were similarly determined. Values of the mean components were then combined for each sector and range and attributed to the appropriate central azimuth, with direction expressed relative to the propagation direction. A wind at the centroid itself was calculated arbitrarily but not unreasonably as the sum of two-thirds of the average of the sector means at the closest range and one-third of the single observed value nearest the centroid. Finally, the mean storm propagation velocity, from 270° at 6 m s^{-1}, was subtracted from all mean winds.

The resulting relative flow at a number of levels is illustrated in Fig. 16. At the surface the relative flow approaches quite uniformly from the right-front sector, with a slight hint of a cyclonic turn in the left-rear sector. The strong mesoscale perturbations observed in the surface wind flow evidently occur on a scale of space or time smaller than those of the storm as a whole. Less than 1 km above, the 900 mb pattern shows a dramatic difference, with overall flow from the right, especially strong inflow at close range in the right-rear sector (where we previously saw maximum instability), and a small cyclonic circulation centered at close range in the left-rear sector. At successively higher levels this circulation becomes more extensive, covering virtually the entire area at 500 mb, where the overall relative flow

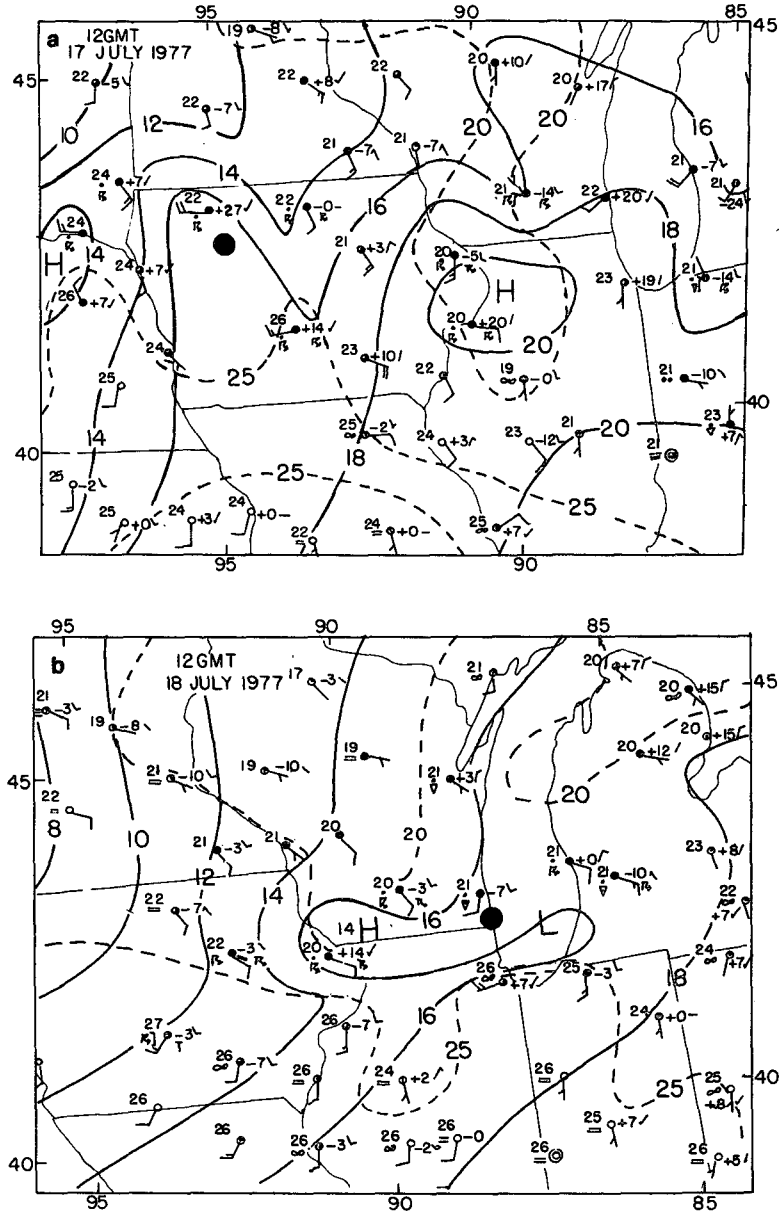

FIG. 7. Surface maps for indicated times, as in Fig. 5. The large dot indicates the estimated position of the centroid of the rainstorm at the time of the map.

is from the rear toward the front of the storm. This change indicates qualitative thermal-wind balance with the cold core below this level seen in Fig. 14. The warm-core character of the system in the upper troposphere is similarly consistent with the change in circulation, as a pronounced anticyclonic circulation at 200 mb replaces the cyclonic one below. The small-scale structure in the right sectors at this level reflects its presence at individual observation times, but its particulars in the composite are doubtless the chance result of a small data sample. In the lower stratosphere, at 100 mb, no residual disturbance can be seen.

5. Mass budget

Despite the differences in structure from sector to sector already described, the circular symmetry suggested by the overall rainfall patterns, by the satellite cloud imagery, and by the composite temperature and wind structure, indicates that study of the mass budget in a cylindrical coordinate system might be fruitful. We have centered such a system on the observed rainstorm.

We have already obtained the distribution of the radial component of wind velocity v_r at a number of radii, as discussed previously. We can obtain the

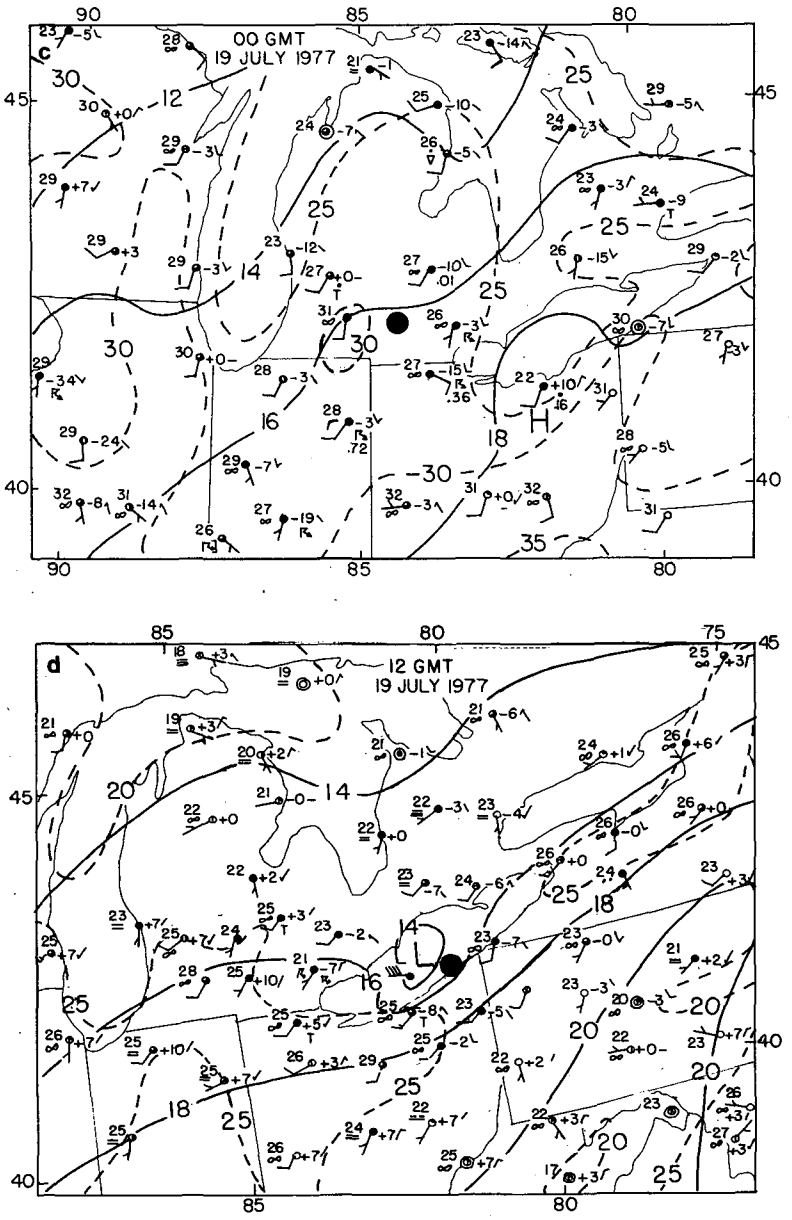

FIG. 7. (*Continued*)

mean "vertical" p velocity ω over an annulus bounded by radii R and $R + \Delta R$ from the integration of the mass continuity equation upward from the surface,

$$\overline{\omega(p)}^{R,R+\Delta R} = \tilde{\omega}_{\text{sfc}}^{R,R+\Delta R} + \int_{p}^{p_{\text{sfc}}} \overline{\nabla \cdot \mathbf{V}}^{R,R+\Delta R} dp,$$

noting that

$$\overline{\nabla \cdot \mathbf{V}}^{R,R+\Delta R} = \frac{(R + \Delta R)\tilde{v}_r^{R+\Delta R} - R\tilde{v}_r^{R}}{\Delta R(R + \Delta R/2)},$$

where the overbar is an area-average over the annulus between radii R and $R + \Delta R$, and the $\tilde{v}_r$ (taken positive outward) are averages around the azimuth rings at R and $R + \Delta R$. The lower boundary condition is $\tilde{\omega}_{\text{sfc}} = 0$ at $p_{\text{sfc}} = 950$ mb.

Results for the inner cylinder of 166 km radius and for three outer annuli bounded by radii of 277, 389, and 499 km appear in Fig. 17, tabulated as uncorrected values. When the integration is carried out to the 100 mb level, the resulting "raw" value of $\tilde{\omega}$ or $\tilde{w}$ is not small. We know that the mean divergence (over the volume) has not been measured correctly. O'Brien (1970) has suggested that this common error often arises from errors in measurement

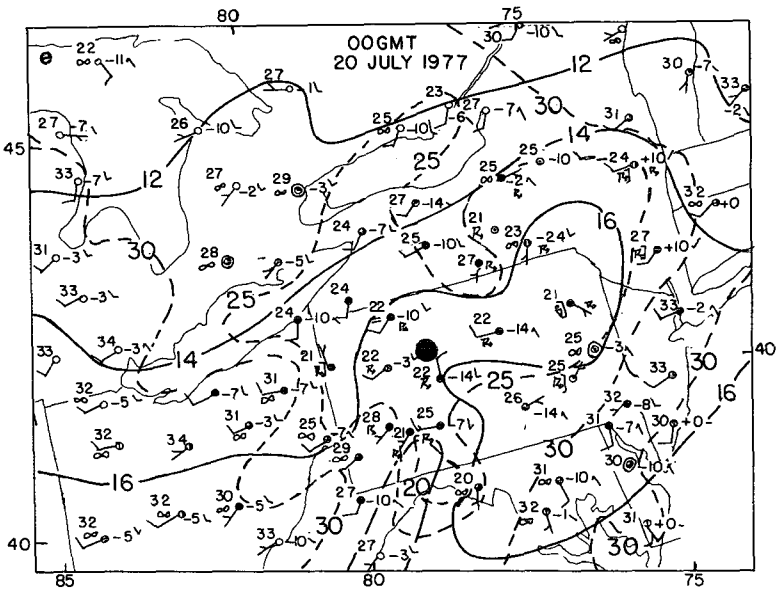

FIG. 7. (*Continued*)

of the balloon position at high levels, when the elevation angle is small, and recommends a height-dependent (or pressure-dependent) correction, increasing upward. In our case large errors occurred even when the winds at upper levels were light, so that the elevation angle cannot have been especially low. Evidently, the errors arise from the presence of small-scale horizontal variability in the wind, not correctly represented in the analysis, the effects of which are not eliminated in the vertical integral. Since the earth's surface is a prominent source of such small-scale variability, it does not seem necessary to apply a larger divergence correction aloft than at low levels. Hence we simply applied constant corrections to all values of v_R, with a magnitude of a few tenths of a meter per second. Vertical profiles of the corresponding corrected values of $\tilde{\omega}$ are plotted in Fig. 17.

A comparison of the tabulated uncorrected values at 100 mb with the much larger corresponding interior extrema together with the simplicity of the uncorrected profiles (not shown), indicate that the results of the computation are credible for the inner cylinder and the outer annuli, and that the main character of final results is not forced by the correction. In the inner cylinder there is substantial ascent, the minimum $\tilde{\omega}$ between 500 and 400 mb corresponding to $\sim$12 cm s^{-1}. There is virtually no vertical motion in the first 50 mb above the surface. Relatively weak descent characterizes the radial interval from 166 to 289 km, maximum values corresponding to 3 or 4 cm s^{-1}. The feeble ascent indicated in the outermost annulus is scarcely 1 cm s^{-1}.

In this azimuthally averaged flow, we can define a "mass flow" streamfunction ψ such that

$$\tilde{v}_r = \frac{1}{r}\frac{\partial \psi}{\partial p}; \quad \tilde{\omega} = -2\frac{\partial \psi}{\partial (r^2)}.$$

The streamfunction was computed by upward integration of $\tilde{v}_r$ from the surface, taken as 950 mb, where ψ was taken to vanish. The result in Fig. 18 shows a section through a torus centered near 500 mb, concentrating intense ascent within 200 km of the centroid with weaker compensating descent out to $\sim$350 km. Inflow does not extend quite to the surface in the innermost 200 km, while the outflow appears to extend to just above the tropopause. A second, much weaker, counterrotating torus appears to be centered near 700 mb at 400 km from the centroid. At 500 km there appears to be weak ascending inflow in the middle troposphere and even weaker quasi-horizontal outflow in the upper troposphere.

This axially symmetric circulation is thus largely self-contained; it communicates only very weakly with the larger scale environment. We may speculate that this secondary circulation would quickly choke the central convection, by warming and drying of the inflowing air, were it not for a substantially stronger primary circulation (cf. Figs. 16a–16c), continually providing a fresh supply of warm, moist unstable air at low levels. We noted before the circumstantial evidence that a reduction in this supply nearly led to the dissipation of the storm on the 18th.

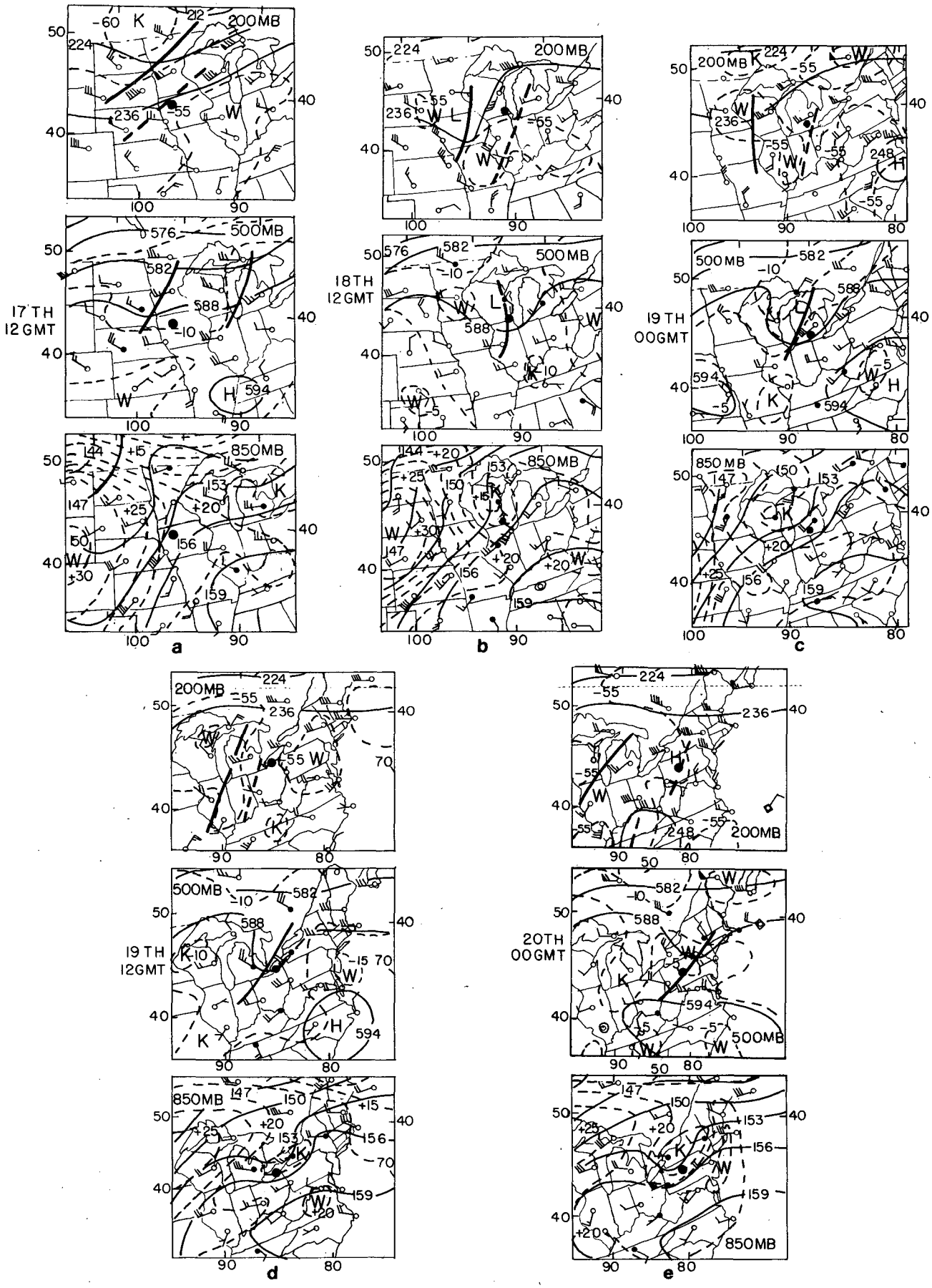
200MB
500MB
850MB
17 TH
12 GMT
18TH
12GMT
19 TH
00GMT
19 TH
12GMT
20TH
00GMT
a
b
c
d
e

We looked for asymmetries by obtaining profiles of ω in the same four azimuthal sectors used before, computed with due allowance for the azimuthal wind components at the sector edges. Results are tabulated and plotted in Fig. 17, along with the aximuthally averaged data. Again, the uncorrected data for the inner cylinder appear credible. They, as well as the corrected values, indicate strong descent in the left-front sector. This is the region where Fig. 16 shows relative airflow leaving the storm system at most levels. Fig. 13 shows this sector to be moister than any other above the 500 mb level, and the satellite imagery in Fig. 2 suggests widespread upper cloudiness here. It is likely that this mesoscale downdraft is driven by evaporative cooling in and beneath a massive anvil in a structure similar to the tropical example described by Zipser (1969). Other azimuthal asymmetries in both the inner cylinder

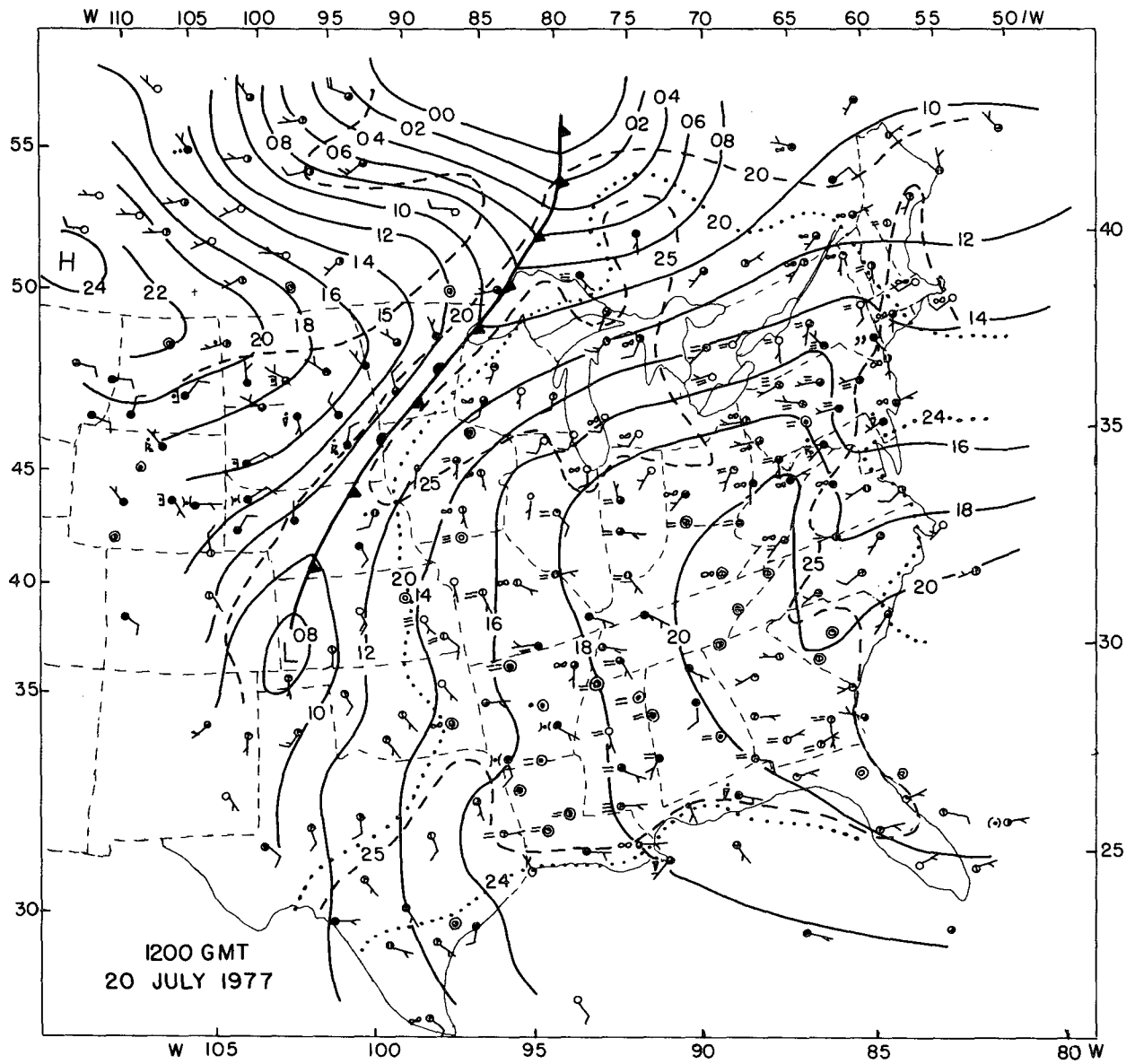

FIG. 9. Surface map, as in Fig. 5, except that the 24°C dew-point isotherm is also shown.

FIG. 8. Upper level charts for indicates times, as in Fig. 6. The large dot indicates the estimated position of the centroid of the rainstorm at the time of the chart. Heavy solid and dashed lines indicate, respectively, positions of selected troughs and ridges in the flow patterns. At 850 and 500 mb, a filled station circle indicated a dew-point depression smaller than 6°C.

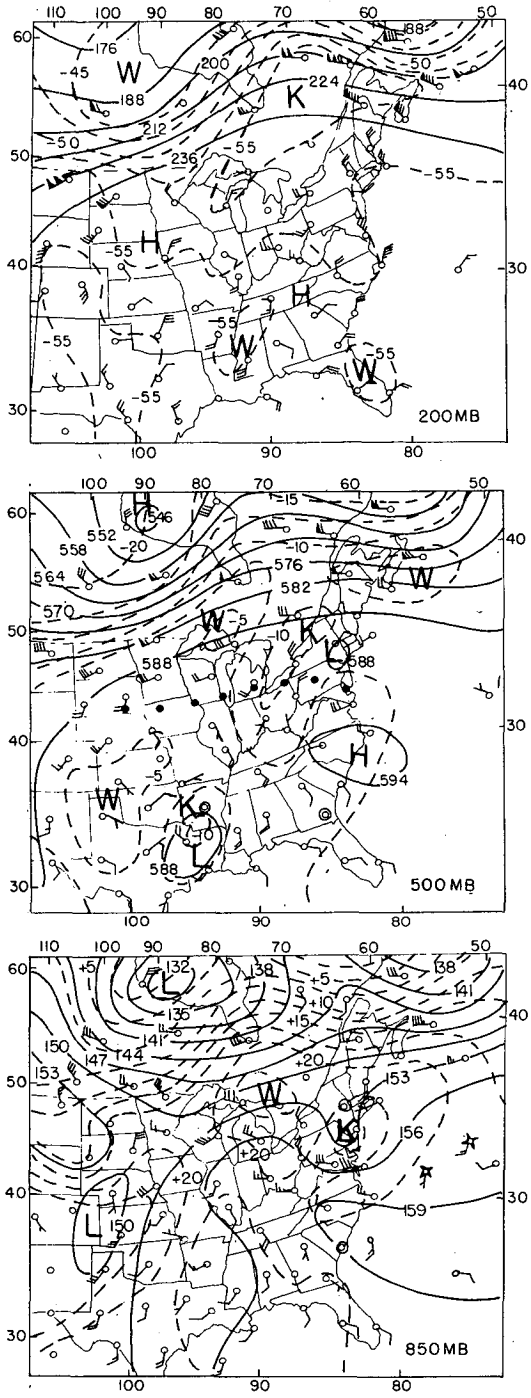

FIG. 10. Upper level charts, as in Fig. 6. The dots on the 500 mb chart are the positions of the centroid of the rainstorm at 12 h intervals from 0000 GMT 17 July to 1200 GMT 20 July.

and the outer annuli are less impressive. The largest, in the right-rear sector of the closest annulus, is the result of a very large correction.

The mean relative vorticity of the azimuthally averaged flow over an annulus, $\bar{\zeta}^{R,R+\Delta R}$, can be obtained from the mean tangential wind components $\tilde{v}_\theta$ since

$$\bar{\zeta}^{R,R+\Delta R} = \frac{\tilde{v}_\theta^{R+\Delta R}(R + \Delta R) - \tilde{v}_\theta^{R} R}{\Delta R(R + \Delta R/2)}.$$

The distribution as a function of p and r^2 is shown in Fig. 19. Strong cyclonic vorticity in the lower and middle troposphere within 150 km of the centroid, capped by intense anticyclonic vorticity in the upper troposphere, resembles the pattern for tropical cyclones, as provided by Frank (1977). Important differences in the present pattern are 1) the failure of strong cyclonic vorticity to reach the ground; 2) lack of an extremely intense inner core; 3) a distinct vorticity minimum in the lower troposphere at 250 km range; and 4) a somewhat lower changeover to anticyclonic vorticity in the upper troposphere. The present pattern appears physically reasonable (aside from small-scale structure near the tropopause, probably arising from sampling); i.e., low vorticity is present where the streamlines are closely spaced in the vertical, suggesting a recent history of divergence, and vice versa. A detailed study of the vorticity budget, however, is beyond the scope of this paper.

Another view of the vertical-motion fields was obtained by calculating weighted mean profiles of ω over triangles enclosing the rainstorm for successive 12 h periods. The triangles, with a sounding station at each vertex, are shown in Fig. 1. We used a modification of Bellamy's (1949) technique, em-

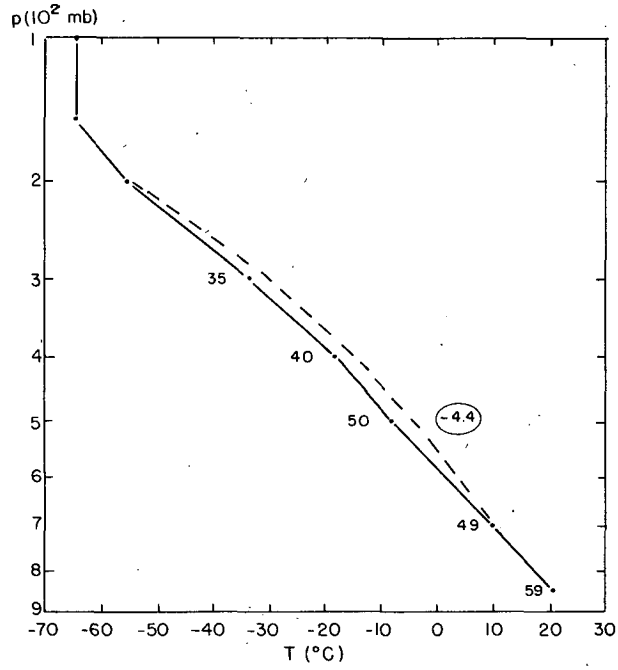

FIG. 11. Mean of 54 soundings within 300 n mi (554 km) of the storm centroid 0000 GMT 17 July–1200 GMT 20 July. Numbers plotted adjacent to data points represent relative humidity. The dashed line represents the moist adiabat for the most buoyant parcel lifted from below 850 mb. The circled number gives the deficit of the ambient 500 mb temperature below the temperature of the lifted parcel.

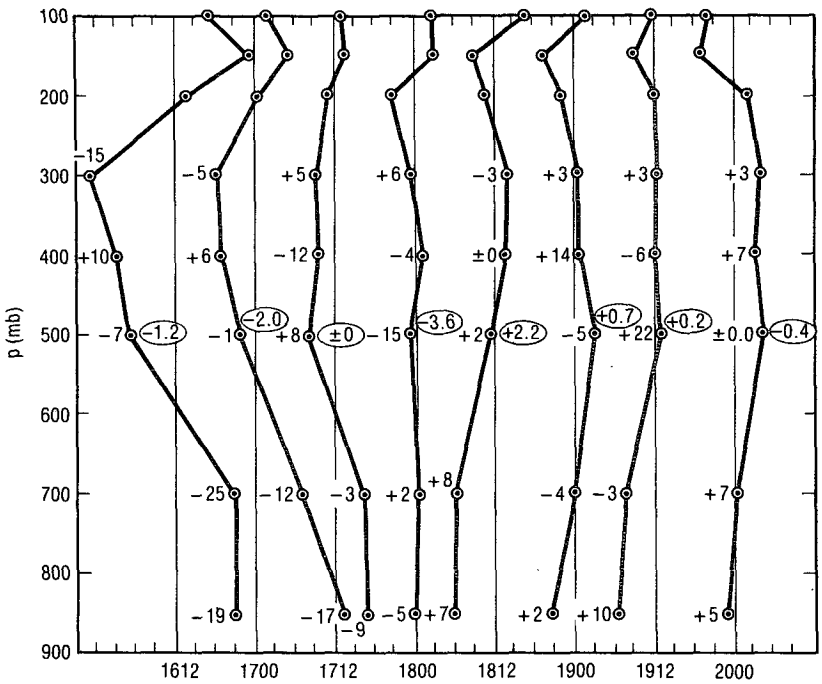

FIG. 12. Deviation of mean soundings for individual times (denoted by date and GMT at the base of the diagram) from the mean shown in Fig. 11. All numerical values are deviations. Tick marks along the horizontal scale represent 1°C.

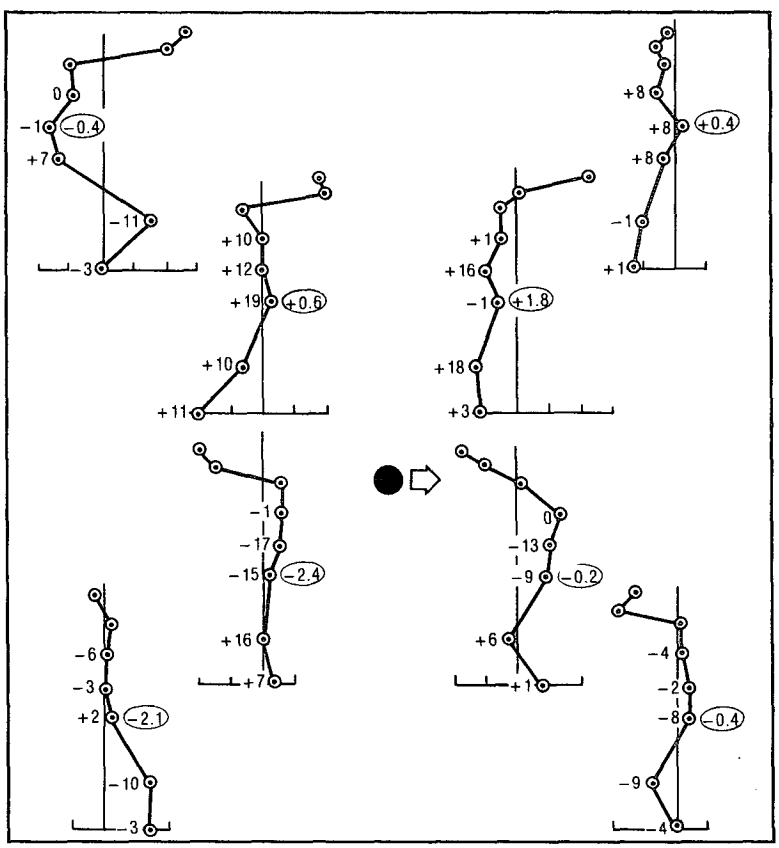

FIG. 13. Deviation of mean soundings, for indicated sectors and ranges, from mean shown in Fig. 11. Convention as in Fig. 12. The position of the storm centroid is shown as a solid dot, with the direction of propagation as indicated by the arrow. The inner range is from 0–180 n mi (332 km); the outer from there to 300 n mi (554 km).

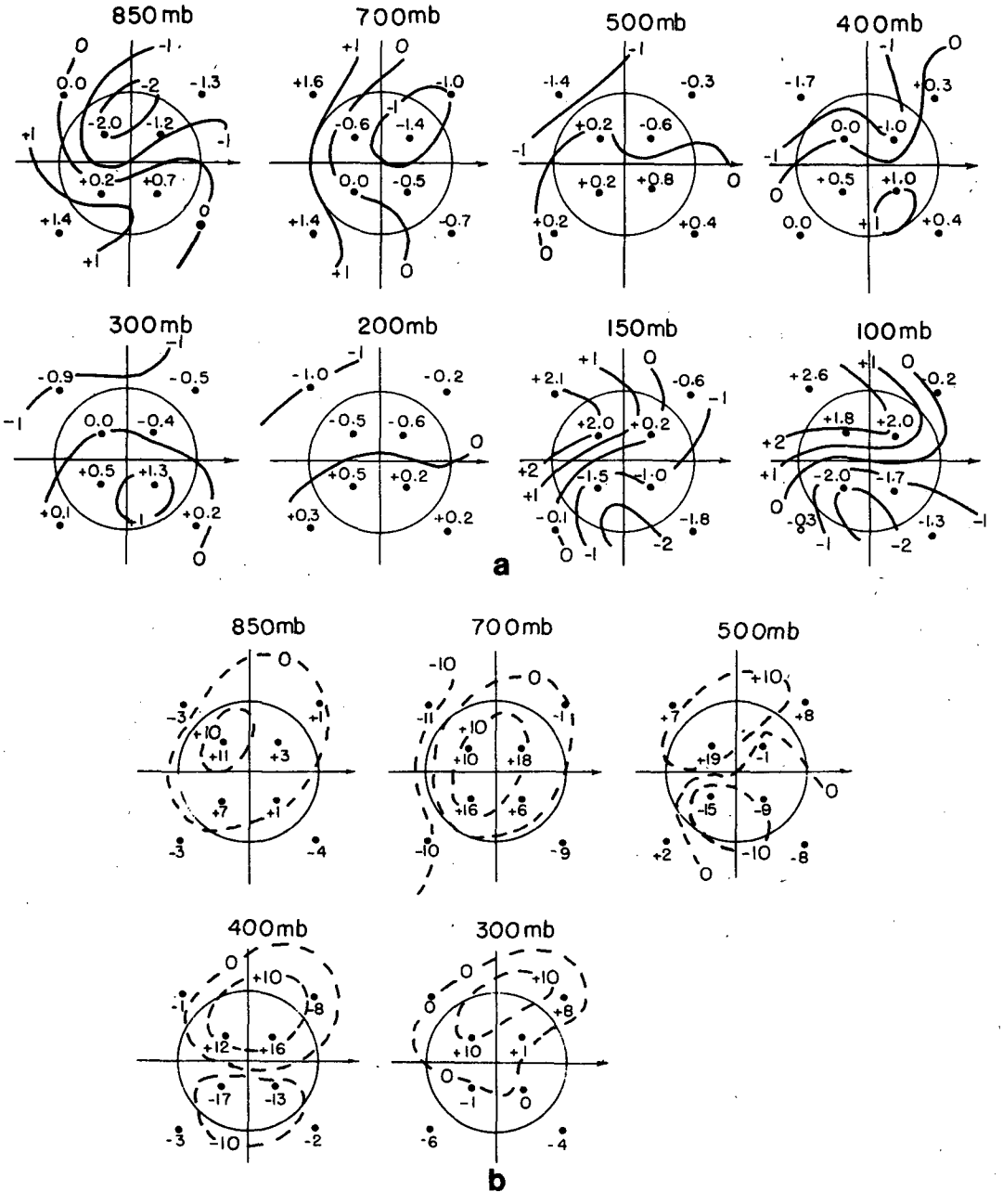

FIG. 14. Display of temperature (solid lines, °C) and humidity (dashed lines, percent) deviations given in Fig. 13, for indicated constant-pressure surfaces.

ploying directly the data at the vertices of the triangles and thus obviating the need for analysis of the fields. In particular, from the integrated form of the mass continuity equation

$$\bar{\omega}(p) = \left(\frac{\partial \bar{p}}{\partial t}\right)_{\text{sfc}} + \sum_{i=1}^{3} \frac{1}{h_i} \int_{p}^{p_i(\text{sfc})} v_{h_i} dp, \qquad (1)$$

where the overbar indicates an average over the area of the triangle, h is the length of the altitude from the vertex to the opposite side, and v_h the wind component at that vertex, outward along h. The effect of flow at the ground across isobaric surfaces is retained by allowing p(sfc), the upper limit of integration, to vary from vertex to vertex. The first term on the right side of (1), though utterly small, was retained because of its utter ease of access. In distinction to the previous calculation, winds from all available levels were used, typically ~35 per

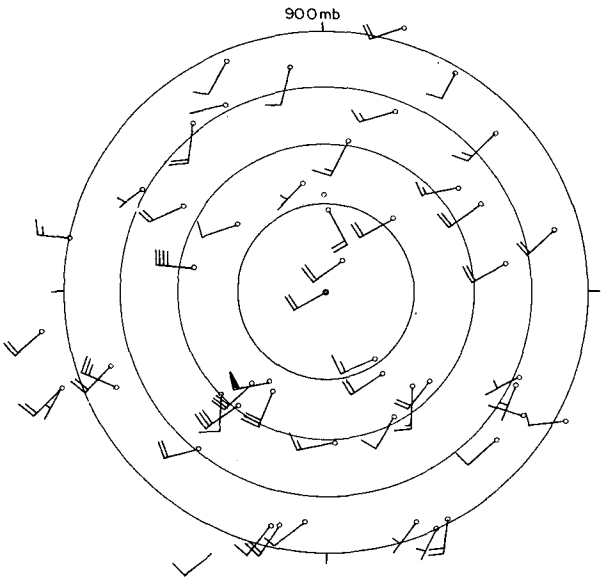

FIG. 15. Composite of winds at 900 mb, plotted in the usual convention and located relative to the position and direction of propagation of the rainstorm centroid (toward the right). Wind directions are shown relative to the propagation direction. A long barb indicates a speed of from 2.5 to 7.5 m s^{-1}.

sounding. From these data, winds were interpolated to levels representing integer multiples of 20 mb, and (1) was integrated upward to 100 mb. Values at 100 mb were unrealistic, as before. Over the 49 triangles used in the calculations, the mean raw value of ω at 100 mb was $+11 \times 10^{-4}$ mb s^{-1}, with a standard deviation of $\pm 84 \times 10^{-4}$ mb s^{-1}, similar to the results obtained earlier for the cylinder and annuli. As before, a uniform correction was made, this time equally to the values of v_h at each vertex. Separate calculations were made for each synoptic time each triangle encompassed part of the 12 h rainstorm.

The triangles, of course, do not coincide exactly with the 12 h rainstorm. To obtain values representative of the rainstorm, we estimated for each 12 h period what fraction of the area enclosed by the 2 mm isohyet fell in each triangle. These fractions were used as weights to be used in combining values for the triangles so as to arrive at a value for the storm. There is a tacit assumption here that all points within a triangle are alike. We have seen, however, that mesoscale ascent accompanies the rainstorm, so that there are probably large mesoscale trends across our triangles, more ascent where it is raining, less where it is not. We did not try to deal with this problem and accept a likely bias in our results toward too little calculated ascent for the rainstorm.

The corrected weighted estimated mean values of mid-tropospheric vertical motion for the rainstorm appear in Table 1, in which 1200 and 0000 GMT

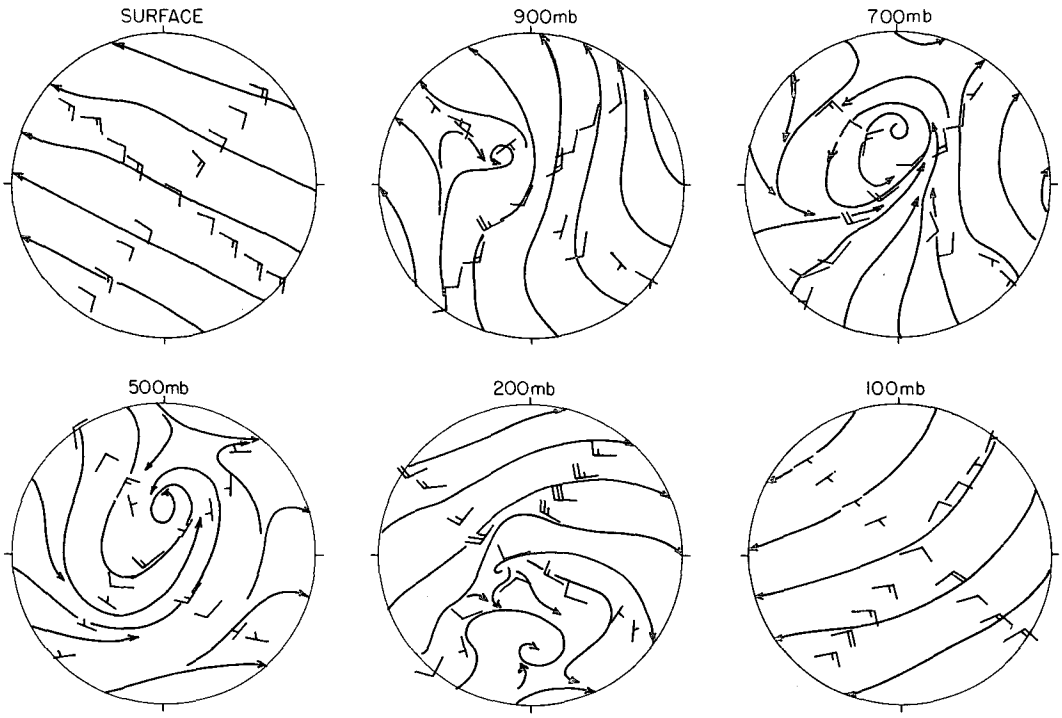

FIG. 16. Mean flow relative to the rainstorm centroid, which is propagating toward the right. Wind plotting convention as in Fig. 15.

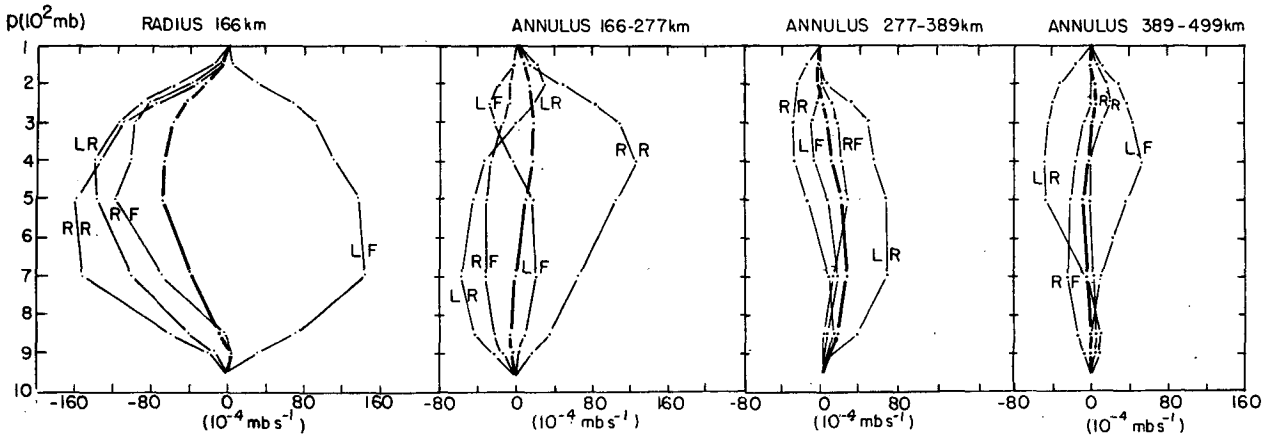

UNCORRECTED	MAX/MIN	100mb
LF	+142(700)	+2
RF	-175(500)	-109
RR	-203(500)	-82
LR	-140(400)	-3
MEAN	-97 (400)	-49

UNCORRECTED	MAX/MIN	100mb
LF	+23(600)	+13
RF	-15(850)	+79
RR	+34(400)	-140
LR	-33(850)	+102
MEAN	+27(300)	+14

UNCORRECTED	MAX/MIN	100mb
LF	+27(700)	+32
RF	+9 (500)	-36
RR	-54(250)	-30
LR	+74(500)	+16
MEAN	+25(700)	-4

UNCORRECTED	MAX/MIN	100mb
LF	+55(400)	+4
RF	-0 (900)	+135
RR	-26(400)	-34
LR	-133(250)	-112
MEAN	-9 (500)	-2

FIG. 17. List of uncorrected p velocities (10^{-4} mb s^{-1}) at 100 mb, with interior extrema and corresponding millibar level of occurrence (in parentheses). Plotted profiles are for corrected values (see text). Mean values for the inner cylinder and the outer annuli are tabulated as such and are illustrated by the heavy profile. Mean values and profiles for four sectors are also indicated.

data are given separately. From 1200 GMT on the 16th until 0000 on the 19th, while the storm is progressing eastward across the north-central United States (cf. Fig. 10), there is descent at 0000 GMT and stronger ascent at 1200. This diurnal variation is produced by the oscillatory behavior of the low-level jet which dominates the central plains during the summer (Bonner, 1968), and which is evidently not qualitatively disrupted by the eastward passage of the convective system through it. In fact, the diurnal oscillation in low-level convergence at the leading edge of the jet must be

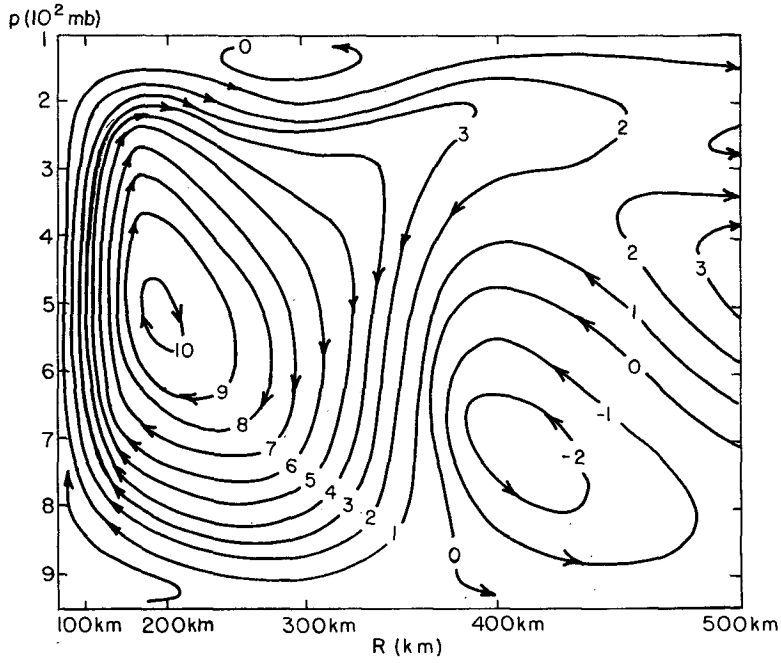

FIG. 18. "Mass-flow" streamfunction ψ (at intervals of 10^7 mb m^2 s^{-1}) for the azimuthally averaged flow about an origin at the centroid of the rainstorm. The sense of the flow is indicated by the arrowheads.

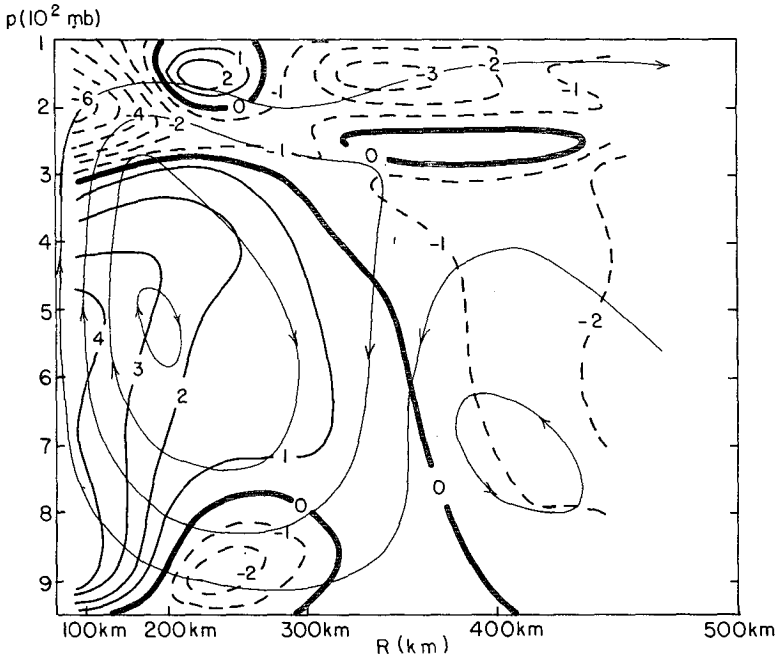

FIG. 19. Relative vorticity of the azimuthally averaged flow at intervals of 1×10^{-5} s^{-1}. The very thin solid lines are selected streamlines from Fig. 18.

responsible for the concentration of heavy rain near dawn and the near cessation of activity in the afternoon during this period, seen in Fig. 3.

Careful study of the data in Table 1 reveals an evident quantitative effect of the storm upon the diurnal variation. Note that the 0000 descent is somewhat stronger at the end of the daytime period, when much of the air over the region of the triangle may not yet have been processed by the storm, than at the beginning of the night period, when most of it has been so processed. Similarly, the 1200 ascent is stronger at the end of the night period and weaker at the end of the daytime period, suggesting also that the effect of the storm is to suppress the amplitude of the diurnal oscillation, although it does not eliminate it. The result is that the storm-scale mean ascent, so far as we can tell by averaging 0000 and 1200 GMT data, virtually disappears during the daytime but is powerful at night. This variation appears to be physically consistent with the tendency of the rainstorm, noted before, to be dispersed during the day and concentrated during the night.

TABLE 1. Mean corrected values of ω (10^{-4} mb s^{-1}) at 500 mb for the area within the 2 mm isohyet.

Period (Date, GMT)	1200 GMT	0000 GMT	Mean
1612–1700 day	−9	+4	−3
1700–1712 night	−33	+3	−15
1712–1800 day	−25	+23	−1
1800–1812 night	−50	+0	−25
1812–1900 day	−16	+7	−5
1900–1912 night	−16	−9	−13
1912–2000 day	−21	−32	−26
2000–2012 night	+3	−32	−14

The average of the two ω values, for each 12 h period, shows an irregular increase to a peak in the period ending at 1200 GMT on the 18th, when the storm is extraordinarily compact and intense (cf. Figs. 1d and 4). The average then decreases sharply as the storm nearly dissipates but then increases, without diurnal oscillation, to another peak at the onset of the Pennsylvania deluge. Finally, there is an indication of rapid cessation of both ascent and heavy precipitation by 1200 GMT on the 20th.

6. Water budget

Having seen that a substantial mass circulation is associated with the storm, we wish to see whether a study of the water transport by this resolvable scale of motion can give insight as to storm processes, even though we grant that important aspects of the rainfall distribution, including indeed the Johnstown disaster, are on a scale much too small to be analyzed with conventional rawinsonde data. We assume that on the scale of the entire convective system, as opposed to the scale of the individual cumulonimbus, the transport of condensed water or ice is a minor factor.

The water vapor budget for a triangle can then be written

TABLE 2. The water vapor budget and its comparison with observed precipitation. Columns 1–4 and $\bar{q}$ are pressure integrals divided by g, expressed as depths of liquid water (mm).

Time period (Date, GMT)	1 $-\bar{q}\overline{\nabla\cdot\mathbf{V}}$	2 $-\bar{\mathbf{V}}\cdot\overline{\nabla q}$	3 $-\partial\bar{q}/\partial t$	4 $-\overline{\nabla\cdot q\mathbf{V}}$	1 + 2 + 3 $\bar{P}-\bar{E}$	4 + 3 $\bar{P}-\bar{E}$	Observed $\bar{P}$	Observed $\bar{q}$
1612–1700	−3.0	+4.1	+0.2	+1.2	1.3	1.4	1.9	27.1
1700–1712	+5.1	+0.2	−1.1	+6.2	4.1	5.1	6.5	33.2
1712–1800	−0.9	+2.5	−0.0	+1.4	1.6	1.4	10.6	40.6
1800–1812	+9.1	+1.1	−0.3	+10.7	9.9	10.4	16.1	39.8
1812–1900	+4.5	−1.6	−0.7	+1.3	2.2	0.6	7.0	39.2
1900–1912	+3.1	+0.2	−2.7	+5.2	0.6	2.5	4.2	39.6
1912–2000	+12.0	+3.0	−5.1	+14.9	9.9	9.8	7.2	43.4
2000–2012	+8.0	+2.0	+1.4	+10.6	11.4	12.0	15.3	46.3
Mean (weighted by area of storm)	+5.0	+1.2	−1.1	+6.1	5.1	5.0	8.8	39.4

$$\overline{P-E} = -\sum_{i=1}^{3}\frac{1}{h_i}\int_{100\text{ mb}}^{\bar{p}_i(\text{sfc})} q_i v_{h_i}\frac{dp}{g} - \frac{\partial}{\partial t}\int_{100\text{ mb}}^{\bar{p}(\text{sfc})}\bar{q}\frac{dp}{g}, \quad (2)$$

where q is the water vapor mixing ratio, and $\bar{P}$ and $\bar{E}$ are precipitation and evaporation at the surface, respectively. Here we assume that no significant flux of water vapor occurs across the 100 mb surface. In fact the flux cannot be measured above the level of the −40°C isotherm, where no humidity observations are available. (We assumed that the relative humidity at the last reported level persists to 100 mb.) Eq. (2) states that the average rate of excess of precipitation over evaporation at the surface over the area of the triangle is provided in part by convergence of the water vapor transport, as expressed by observed transports at the vertices, and in part by a reduction in the amount of water vapor stored in the atmosphere.

The convergence of the transport, $-\nabla\cdot q\mathbf{v}$, can be decomposed in principle into area averages of horizontal moisture advection, $-\overline{\mathbf{v}\cdot\nabla q}$, and of convergence in the presense of water vapor, $-\overline{q\nabla\cdot\mathbf{v}}$. We, however, could calculate only $-\bar{\mathbf{v}}\cdot\overline{\nabla q}$ and $-\bar{q}\overline{\nabla\cdot\mathbf{v}}$ from the available data. Their sum differs from the first term on the right side of (2) because the latter takes account of correlation between q and v_h at the three vertices.

The required integration in time over a 12 h period was accomplished, admittedly crudely, by averaging the convergences and advections computed at the beginning and end. To obtain values for the storm area we obtained weighted averages for the constituant triangles, as described for the mass budget. We used corrected values for the convergences, as described before. (The advection term is not affected by the uniform correction.)

The mean results in Table 2 show (i) that low-level mass convergence in the presence of large values of water vapor with compensating mass divergence aloft in regions of little water vapor is the dominant effect, (ii) that neither moist advection nor the change in storage are negligible, but they approximately balance each other, (iii) that the correlation of q and v_h has little systematic effect (since the sum of columns 1–3 nearly equals the sum of columns 3 and 4) (iv) that surface evaporation contributes importantly to precipitation, and (v) that a little more than a fifth of the stored water vapor falls as precipitation in 12 h. Of each 100 units of water vapor made available to the storm, our calculations show that 51 come from storm-scale mass convergence, 12 from storm-scale moist advection, and 37 from surface evaporation. Of this total, 11 units are used to moisten the atmosphere and 89 fall as precipitation. As mentioned earlier, we may have understated the contribution to mass convergence and attributed too much to surface evaporation, but it seems unlikely that evaporation is unimportant. A separate calculation of the water budget over the larger area encompassing the entirety of the triangles, required comparable amounts of evaporation. Our results seem comparable to those of Thompson *et al.* (1979) for precipitation in synoptic-scale waves in the tropical Atlantic during Phase III of GATE. In the wave trough, where precipitation is at a maximum (at a value 125% of ours), they find that of 100 units of water vapor made available, 83 come from moisture convergence (compared to our 63 units) and 17 come from surface evaporation; that 6 are used to moisten the atmosphere while 94 precipitate.

An examination of values for the individual periods shows prominent opposing diurnal oscillations in the mass-convergence and advection effects while the storm traverses the northern plains, reflecting the diurnal oscillations in storm-scale vertical motion discussed earlier. Cursory examination of the low-level jet shows strong convergent southwesterlies with little moisture advection at 1200 GMT, and

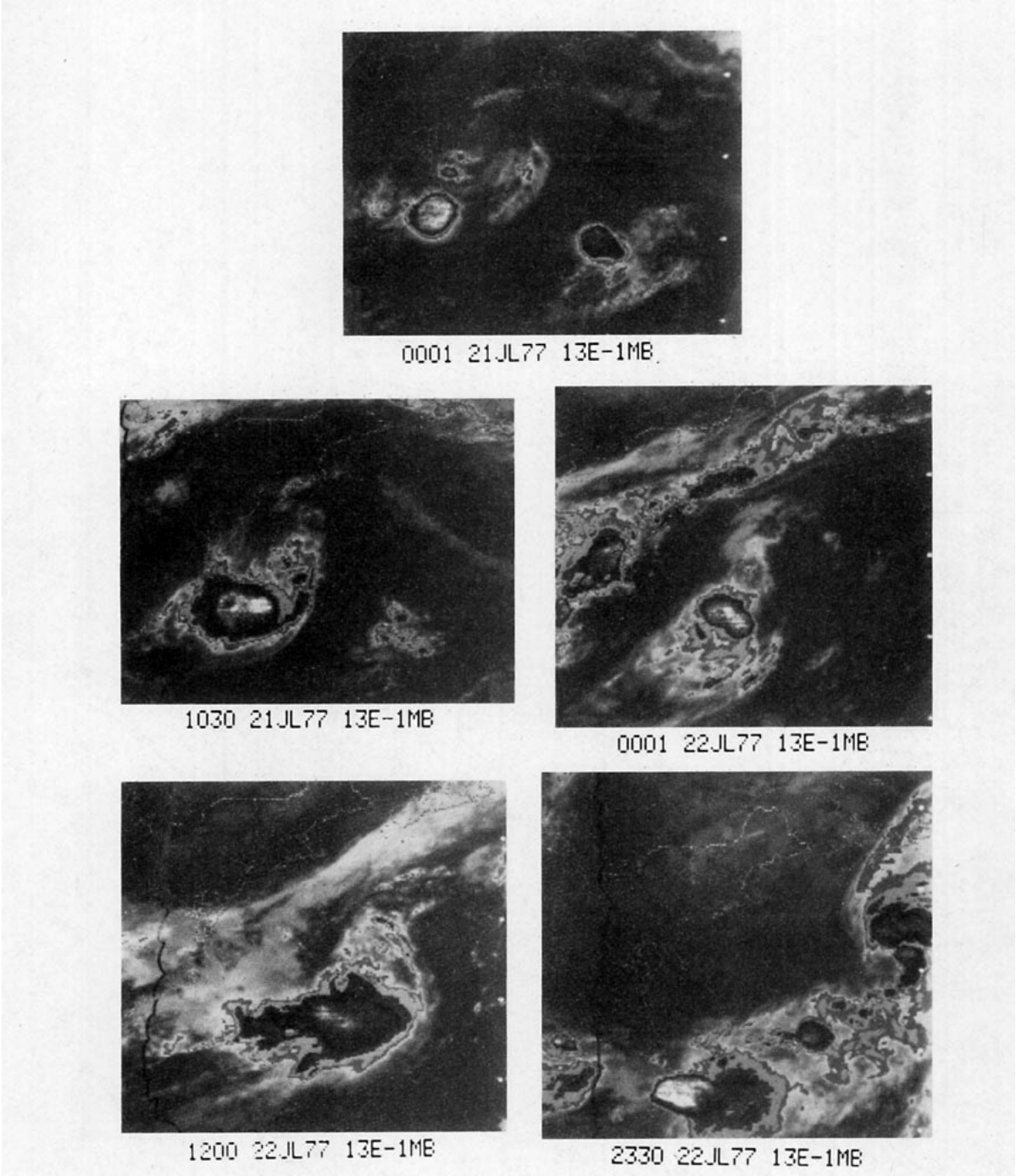

FIG. 20. GOES-E satellite IR imagery for indicated times.

weaker divergent southerlies with relatively strong moist advection at 0000 GMT. Evidently, these characteristics dominate the night and day periods, respectively, for reasons discussed earlier. The near balance in the mean between advection and local change is not seen during the individual periods, unfortunately. Neither do we find a good correlation between the mass-convergence effect and rainfall, as Krishnamurti *et al.* (1980) did during GATE Phase III. Finally, by comparing values of $\bar{P}$ and $\overline{P-E}$, we find little difference of implied evaporation from day to night, confirming our suspicion that we have overestimated it.

Of course, there is the further question whether the 12 h average of the moisture convergence is adequately represented by measurements at 12 h

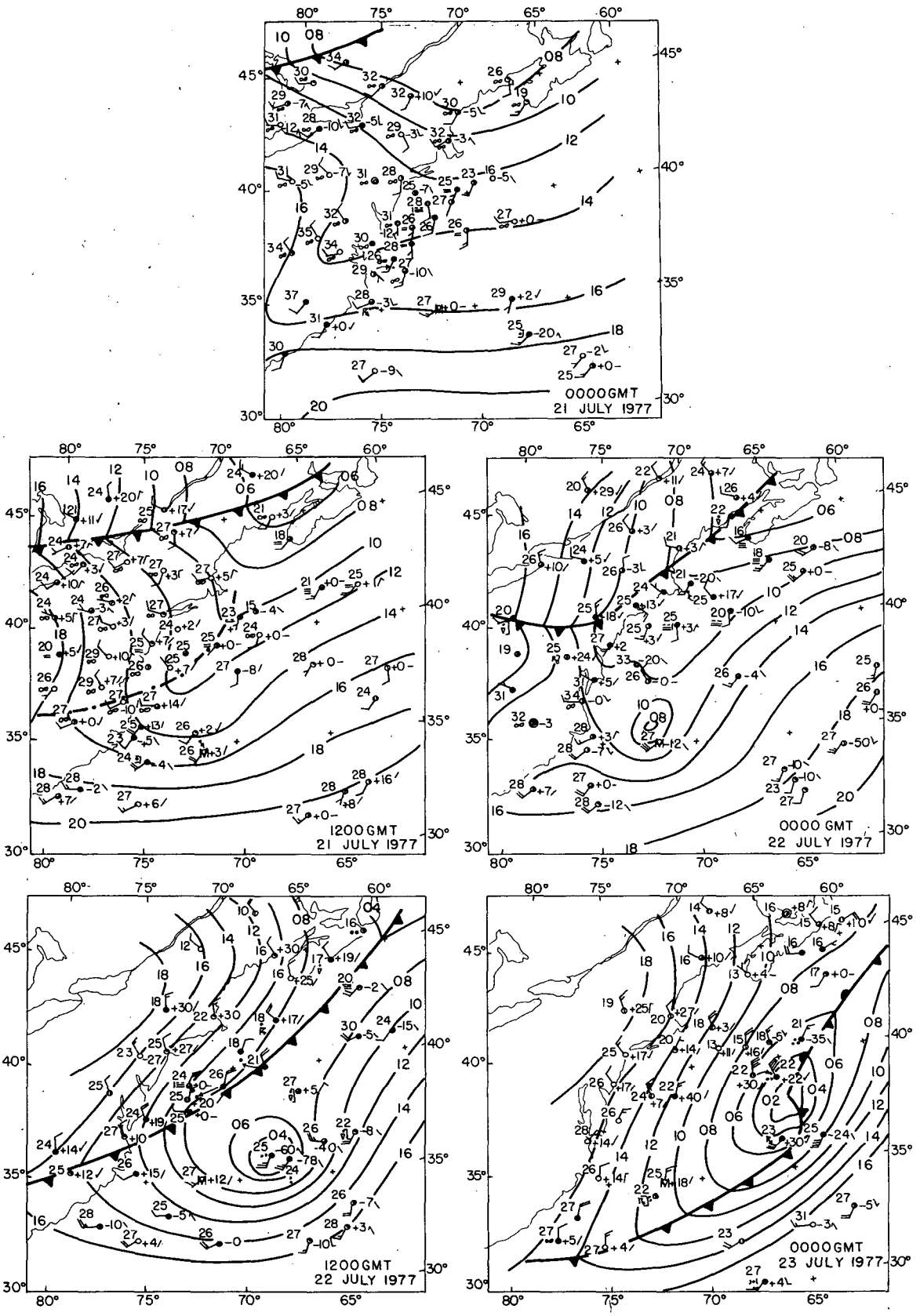

FIG. 21. Surface maps as in Fig. 5.

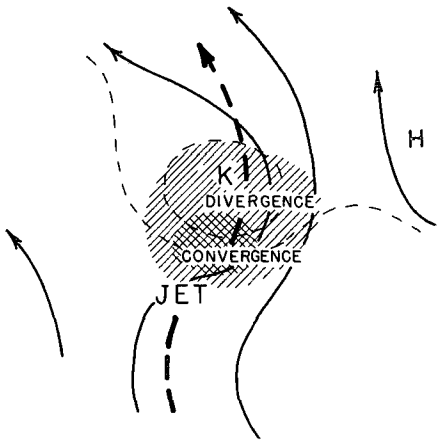

FIG. 22. Schematic diagram of proposed mechanism for the long-lived convective storm. Thin lines represent streamlines of relative geostrophic flow and the heavier dashed lines the relative actual flow. Dashed lines are isotherms defining the cool pool, centered at K. Hatching shows the area of rain, cross-hatching indicating the heaviest.

intervals, between which there are large changes. Rasmussen (1968), however, noting the same diurnal variation in moisture convergence, was nevertheless able to use data at 0000 and 1200 GMT to make satisfactory mean annual and monthly water-budget calculations. Moreover, correlations between $\bar{P}$ and diagnosed $\overline{P-E}$ for the eight time periods are encouraging. The sum of columns 1–3 in Table 2 correlates 0.73 with $\bar{P}$, while the correlation between the sum of columns 3 and 4 and $\bar{P}$ is 0.70. An *a posteriori* justification for correcting the winds, to remove the spurious mean divergence, is provided by a correlation of only 0.54 between the uncorrected values of $\overline{P-E}$ (not shown) and $\bar{P}$.

7. An oceanic postscript

Passage across the Atlantic coast does not mark the end of the convective system, as can be seen in Fig. 20 at 0000 GMT on the 21st. Remnants of the Pennsylvania system lie off the mid-Atlantic states and a well-defined new patch of cold cirrus cloud marks an area of vigorous convection on the North Carolina coast. This area drifts southeastward and expands over the next 36 h, finally merging by 2330 GMT 22 July with a band of clouds associated with the eastward-moving cold front seen in Fig. 9.

The surface maps for this period appear in Fig. 21. The trough in the lee of the Appalachians develops eastward over the Gulf Stream, where it becomes concentrated into a small vortex, of tropical-storm intensity. This vortex quickly merges with the circulation of the approaching cold front and moves rapidly northeastward toward Newfoundland. The vortex forms and remains near the northern edge of the convective cluster until merger with the cold front.

Sanders (1972) has documented another case in which the passage of a convective complex offshore from the mid-Atlantic states was accompanied by the growth of a vigorous circulation over the ocean, but in that instance the pattern was one of multiple disturbances rather than the single vortex seen here. In another example, the explosive development of the cyclone which damaged the *Queen Elizabeth II* in September 1978 has recently been shown by Gyakum (1980) to have started just northwest of a prominent convective cluster resembling the one illustrated in Fig. 15. Thus the accumulating evidence suggests that the midlatitude convective system will develop a strong associated surface circulation over warm water. The vorticity distribution in Fig. 19, after all, indicates that only the lowest 50 mb requires spinup. The inhibition over land may be due to the relatively large surface stress or to the lack of sufficient surface heating to prevent the accumulation of cool stable air.

8. The role of the cool pool

We saw in Fig. 8b–8e, 10 and 14, a pervasive pool of cool air at 850 and 700 mb just north of the centroid of the rainstorm. Surface maps for the same times show a less well-organized region of cool air in the precipitation region. This coolness is maintained, one way or another, by the convection, and is hydrostatically responsible for the high vorticity seen near the storm in Figs. 8, 10, 16, and 19. From 900 to 700 mb, the pool is bounded on the south by a narrow zone of strong wind. The entire complex moves along at ~6 m s^{-1}, nearly the speed of the area-averaged flow at 500 mb.

Since the speed at this low-level jet core ranges from 15 to 20 m s^{-1}, the air in the core and in the high-vorticity region just to its north, and hence near the centroid of the rainstorm, must overtake the system from the southwest and leave it toward the northeast, as indicated schematically in Fig. 22. Vorticity in the air must then spin up by convergence on approaching from the west and spin down by divergence on leaving. Air entering the jet region (if parcel accelerations are produced by the local horizontal pressure-gradient force) must cross height contours toward lower values. Air leaving the core must cross the contours toward higher height. Mid-tropospheric vertical motions shown in Fig. 17 are consistent with the suggested lower convergence and divergence patterns, while there is evidence of cross-contour flow in the suggested sense at 850 mb in Figs. 8b, 8d and 8e. A similar kind of transverse circulation has been proposed by Uccellini and Johnson (1979) as a factor in the generation of severe convection, but in their case, unlike ours, a key role is played by a jet streak in the upper troposphere.

We speculate that the vertical motions enhance the convection, that the convection reinforces the

cool pool, and that the pool reinforces the lower tropospheric jet in a system of positive feedback. We grant that the proposed mechanism is *ad hoc*, but suggest that continuing evidence should be sought in other convective systems, which Maddox (1980) finds so numerous in the central United States in the summer. (Routine soundings should be adequate for some purposes, although increased spatial and temporal coverage is highly desirable.)

The balance must be a fine one, however, because most of Maddox's cases do not persist as long as this one which ultimately came to Johnstown. This one, moreover, was temporarily dispersed over the Great Lakes region but managed through the agency of the continuing mid-tropospheric vorticity maximum to become reorganized, to devastating effect in western Pennsylvania. The mechanism of these changes of structure remains obscure.

9. Conclusions

We find that the extraordinarily heavy rain which produced the flash floods near Johnstown on the night of 19–20 July 1977 was part of a larger convective complex which originated in South Dakota nearly four days earlier. Soon after organization, perhaps in association with an upper tropospheric jet streak of the type analyzed by Uccellini and Johnson (1979), the complex became closely associated with a mid-tropospheric vorticity maximum, lying above a pool of relatively cool air in the lower troposphere, embedded in a widespread warm, humid and unstable air mass.

Convergence at the southern and western edge of this cool pool, together with surface evaporation, provided adequate moisture for the storm, with convection producing the precipitation on relatively small scales despite lack of large-scale saturation. We heuristically propose a mechanism in which a transverse circulation in the lower tropospheric jet bounding the cool pool on the south and west acts as a positive feedback between the convection and the warm moist air feeding it. We are unable to define specifically the conditions in which the feedback system is maintained, nor are we able to account quantitatively for the exceptionally heavy amounts of precipitation in the vicinity of Johnstown.

Apparently, this mechanism is readily altered when the system passes over a warm water surface. There is a tendency toward rapid spinup of the circulation in the surface layer, presumably accompanied by warming of the troposphere. Thus the resemblance of the overland convective system to the young tropical cyclone, which was hitherto considerable except in the lowest 50 mb, becomes nearly complete.

Acknowledgments. The authors are grateful to Bob Maddox and Ray Hoxit of NOAA Office of Weather Research and Modification (OWRM) for providing rawinsonde data and to Charles Dobbs of MIT for assistance with the calculations. They have benefited from discussions of various aspects of convection with John Brown and Ed Zipser, of the National Center for Atmospheric Research[1], Mike Fritsch of OWRM and Fred Carr of the University of Oklahoma. They wish to thank Isabelle Kole, Virginia Mills and Joel Sloman of MIT, for preparation of the figures and manuscript. This research was supported by the National Science Foundation under Grants ATM 7800531 and ATM 7815942.

REFERENCES

Bellamy, J. C., 1949: Objective calculations of divergence, vertical velocity and vorticity. *Bull. Amer. Meteor. Soc.*, **30**, 45–49.

Bonner, W. D., 1968: Climatology of the low-level jet. *Mon. Wea. Rev.*, **96**, 833–850.

Frank, W. M., 1977: The structure and energetics of the tropical cyclone. I. Storm structure. *Mon. Wea Rev.*, **105**, 1119–1135.

Fritsch, J. M., and C. F. Chappell, 1980: Numerical prediction of convectively driven mesoscale pressure systems. Part I: Mesoscale model. *J. Atmos. Sci.*, **37**, 1734–1762.

Gyakum, J. R., 1980: On the evolution of the QEII storm. *Preprints Eighth Conf. Weather Forecasting and Analysis*, Denver, Amer. Meteor. Soc., 23–28.

Hoxit, L. R., R. A. Maddox, C. F. Chappell, F. L. Zuckerberg, H. M. Mogil, I. Jones, D. R. Greene, R. E. Saffle and R. A. Scofield, 1978: Meteorological analysis of the Johnstown Pennsylvania flash flood, 19–20 July 1977. NOAA Tech. Rep. ERL 401-APCL 43, 71 pp.

Krishnamurti, T. N., Y. Ramanathan, H.-L. Pan, R. J. Pasch and J. Molinari, 1980: Cumulus parameterization and rainfall rates I. *Mon. Wea. Rev.*, **108**, 465–472.

Maddox, R. A., 1980: Mesoscale convective complexes. *Bull. Amer. Meteor. Soc.*, **61**, 1374–1387.

——, C. F. Chappell and L. R. Hoxit, 1979: Synoptic and meso-α scale aspects of flash flood events. *Bull. Amer. Meteor. Soc.*, **60**, 115–123.

O'Brien, J. J., 1970: Alternative solutions to the classical vertical velocity problem. *J. Atmos. Sci.*, **9**, 197–203.

Rasmussen, E. M., 1968: Atmospheric water vapor transport and the water balance of North America. II. Large-scale water balance investigations. *Mon. Wea. Rev.*, **96**, 720–734.

Sanders, F., 1972: Meteorological and oceanographic conditions during the 1970 Bermuda Yacht race. *Mon. Wea. Rev.*, **100**, 597–606.

Scofield, R. A., 1978: Using satellite imagery to estimate rainfall during the Johnstown rainstorm. *Preprints Conf. Flash Floods: Hydrometeorological Aspects*, Los Angeles, Amer. Meteor. Soc., 181–189.

Thompson, R. M., Jr., S. W. Payne, E. E. Recker and R. J. Reed, 1979: Structure and properties of synoptic-scale disturbances in the intertropical convergence zone of the eastern Atlantic. *J. Atmos. Sci.*, **36**, 53–72.

Uccellini, L. W., and D. R. Johnson, 1979: The coupling of upper and lower tropospheric jet streaks and implications for the development of severe convective storms. *Mon. Wea. Rev.*, **107**, 682–703.

Zipser, E. J., 1969: The role of unsaturated convective downdrafts in the structure and rapid decay of an equatorial disturbance. *J. Appl. Meteor.*, **8**, 799–814.

[1] The National Center for Atmospheric Research is supported by the National Science Foundation.